A theoretical and experimental study of the near edge X-ray absorption fine structure (NEXAFS) and X-ray photoelectron spectra (XPS) of nucleobases: thymine and adenine

O. Plekan [1,2], V. Feyer [3], R. Richter [1], M. Coreno [3], M. de Simone [4], K.C. Prince [1,4 *], A. B. Trofimov [5], E. V. Gromov [5,6], I. L. Zaytseva [5], J. Schirmer [6]

[1] *Sincrotrone Trieste, in Area Science Park, I-34012 Basovizza (Trieste), Italy*

[2] *Permanent address: Institute of Electron Physics, 88017 Uzhgorod, Ukraine*

[3] *CNR-IMIP, Montelibretti (Rome), I-00016 Italy*

[4] *Laboratorio Nazionale TASC, INFM-CNR, 34012 Trieste, Italy*

[5] *Laboratory of Quantum Chemistry, Irkutsk State University, Karl Marx str. 1, 664003 Irkutsk, Russian Federation*

[6] *Theoretische Chemie, Physikalisch-Chemisches Institut, Universität Heidelberg, Im Neuenheimer Feld 229, D–69120 Heidelberg, Germany*

Abstract.

The core level electron excitation and ionization spectra of thymine and adenine have been investigated by photoabsorption and photoemission spectroscopy, and the results interpreted by means of *ab initio* calculations using the second-order algebraic-diagrammatic construction (ADC(2)) method for the polarization propagator and the fourth-order ADC method (ADC(4)) for the one-particle Green's function. The photoabsorption spectra are dominated by transitions from core levels to unoccupied π states, but also show clear structures due to Rydberg transitions. The calculated spectra are in good agreement with the experimental results, and many of the observed structures are assigned.

1. Introduction.

Nucleobases are fundamental building blocks of life, and their physical chemistry has been extensively studied both experimentally and theoretically. Gas

phase studies of these compounds provide an opportunity to examine the spectra of these molecules in the absence of solvation effects and thus obtain detailed and precise information. The compounds of interest here, thymine and adenine (Fig. 1), have been studied by valence band photoemission (see reference [1] and references therein). We are not aware of any gas phase core level photoemission spectra of these molecules, although data exist for some related compounds such as 2-hydroxypyridine [2]. The core level binding energies of thymine and adenine have been calculated by Takahata et al [3] using density functional theory (DFT), and the N K edge core level photoabsorption spectrum of adenine has been calculated by Mochizuki et al [4] using the Hartree-Fock static exchange (HF-STEX) method [5]. The C K edge NEXAFS of thymine and adenine have been measured in the solid state by Moewes et al [6], and compared with spectra calculated for the free molecules using the improved virtual orbitals (IVO) method involving relaxed Hartree-Fock (HF) potentials. They also reported C edge resonant X-ray emission spectra of thymine. Other experimental studies include infrared spectroscopy of thymine in He nanodroplets [7], while Colarusso et al [8] measured the gas phase infrared spectrum of thymine and adenine. They found that a single tautomer of each compound exists at their experimental temperatures of 200 to 325 °C, a result in accordance with previous low temperature matrix isolation studies.

Theoretical studies have sought to calculate accurately the bonding geometry and total energies of DNA bases. Fonseca Guerra et al [9] calculated the relative stabilities of tautomers of adenine, and the valence ionization energies, and Scanlan and Hillier [10] also studied the tautomerism of thymine theoretically. The ground state molecular structures of thymine and adenine have been calculated by Dolgounitcheva et al [11, 12] in the context of their theoretical study of the ionization energies in these molecules. Also, recent theoretical studies [13-16] have dealt with tautomerism, gas phase structure and stability of thymine and adenine.

Here we report a joint theoretical and experimental investigation of the core level photoemission and photoabsorption spectra of the nucleobases thymine and adenine.

2. Experimental methods.

The samples were obtained from Sigma–Aldrich in the form of crystalline powder with minimum purity of 99% and used without any further purification. They

were evaporated from a home-built furnace with an effusive nozzle and were checked before the experiment using photoionization mass spectroscopy [17], to ensure that there are no effects due to thermal decomposition of the product. Since we use an effusive nozzle instead of a gas cell, we minimize the possibility of spurious effects such as reactions on the surface of the cell, photolytic effects, or concentration of reaction products in the cell. Evaporation temperatures were 393 K for thymine and 448 K for adenine.

The photoemission spectra were taken at the Gas Phase Photoemission beamline, Elettra, Trieste [18], using a 150 mm hemispherical electron energy analyser, equipped with 6 channel electron multipliers. The electron analyzer was mounted with its axis at a forward scattering angle of 54.7° with respect to the electric vector of the linearly polarized light, and in the same plane as the beam propagation direction. In this geometry the electron analyzer is set at the (pseudo) magic angle and measurements should be insensitive to the photoelectron asymmetry β parameter. Valence spectra were taken at 99 eV photon energy to check the quality of the samples and were consistent with those published by Trofimov et al [1], apart from differences in relative peak intensity due to photon energy and geometry differences. The C 1s, N 1s and O 1s core photoemission spectra were taken at 382, 495 and 628 eV photon energy respectively and the binding energy calibrated to the 1s energies of N_2 and CO_2 [19, 20]. The spectra were measured with a total resolution (photons+analyser) of 0.45, 0.57, 0.59 and 0.53 eV at hν=99, 382, 495 and 628 eV, respectively.

The photoabsorption spectra were acquired by measuring the total ion yield with a channel electron multiplier placed near the ionization region. The resolution was 70, 60, and 100meV at the C, N and O edges, respectively.

2.1. Computational details: Photoabsorption.

The excitation energies and photoabsorption intensities of (vertical) K-shell transitions in thymine and adenine (Fig. 1) were computed using the second-order algebraic-diagrammatic construction (ADC(2)) scheme for the polarization propagator [21, 22] specialized to the case of K-shell excitations by means of the additional core-valence separation (CVS) approximation [23]. The ADC(2)/CVS method has been

used previously in various applications and the reader is referred to Refs. [24-30] for details of such calculations.

In brief, the ADC(2) method treats all effects relevant to electron excitation such as relaxation, polarization and electron correlation through second-order in the Coulomb repulsion. The ADC(2) excitation energies Ω_n and dipole moments T_n for the vertical transitions from the ground state $|\Psi_0\rangle$ to excited state $|\Psi_n\rangle$ allow one to evaluate dipole oscillator strengths f_n which serve as a measure of photoabsorption intensities [21, 22]. In the ADC(2)/CVS approach all K-shell excited states associated with a given atomic species (e.g., 1s excited states of carbon) are treated on the same footing. The "extended" version of the ADC(2) scheme [21, 22] used in the present work accounts for all singly and doubly excited configurations involving a single core-level vacancy.

The ADC(2)/CVS method renders a highly consistent and balanced description of the K-shell excitation manifold, and provides a reliable interpretation of the excitation spectra. Even though the agreement between the calculated and experimental excitation energies is not quantitative, the error is usually very uniform [28-30] so that the relative energies and the correspondingly shifted theoretical spectral profiles agree very well with experiment.

It should be noted that the ADC(2) method differs considerably from other theoretical approaches used to simulate NEXAFS spectra and soft X-ray absorption spectra (XAS) of larger molecules (see, for example, Refs. [3, 4, 6, 31-34]). The latter methods are normally based on a one-particle description of the excited electron in the field of the core-hole ion, such as in the Hartree-Fock static exchange (HF-STEX) scheme of Ågren et al [5] or the DFT-TP approach [32] combining density-functional theory (DFT) with the transition operator or transition potential (TP) method [35, 36]. While the expense of these computational schemes is relatively low, an obvious drawback is the fact that the (second-order) polarization effect, that is, the response of the ionic core to the presence of an excited electron, is neglected. Moreover, the necessity to start from a localized representation of the ionic core-hole states may cause problems in systems with equivalent 1s orbitals.

2.2. Computational details: Photoionization.

The K-shell photoionization spectra were computed using the fourth-order algebraic-diagrammatic construction (ADC(4)) scheme for the one-particle Green's function [37-39], also employing the core-valence separation approximation [23, 40] (the theoretical aspects of the ADC(4)/CVS approach are discussed in Refs. [41, 42], while applications to various systems can be found in Refs. [40, 42, 43]).

As in the case of excitation, the ADC(4) method accounts for all effects relevant to ionization (relaxation, ground- and final-state electron correlation). The fourth order treatment enables a more accurate description of the K-shell spectrum. The calculations comprise the main photoelectron lines originating from one-hole (1h) configurations and, moreover, photoelectron satellites originating from two-hole one-particle (2h-1p) and three-hole two-particle (3h-2p) electronic configurations.

The calculated spectrum is described in terms of the (vertical) ionization energies Ω_n and so-called spectroscopic factors P_n given as the squared moduli of the matrix elements $\left\langle \Psi_n^{N-1} \middle| c_p \middle| \Psi_0 \right\rangle$. Here c_p is the annihilation operator (of second quantization) associated with the core orbital φ_p. Usually there is only single core orbital associated with a specific final ionic state $\left| \Psi_n^{N-1} \right\rangle$, and in this case the spectroscopic factors are a measure of the relative spectral intensity [37-40].

Compared to configuration interaction (CI) treatments of similar accuracy, the secular matrices of the ADC methods are smaller (more compact) [21, 22, 37-40, 44]. Moreover, in contrast to (truncated) CI expansions, the ADC methods are size-consistent [45], which is an essential prerequisite for the application to larger molecules such as the nucleobases studied here.

2.3 Computational details: general.

The ground-state geometrical parameters of thymine and adenine (Fig. 1) were obtained by means of a geometry optimization procedure using the DFT method (at the B3LYP level) [46] and 6-311G** basis sets [47]. The DFT calculations were carried out using the GAUSSIAN package of programs [48].

For thymine only diketo tautomers (Fig. 1) were considered in the present work, as there are no other tautomers which are close to them in energy (see, for example, Refs. [7, 12, 13, 49] and literature cited therein). Further, with respect to the methyl

group rotation only the *cis* conformer was considered: it is characterized by the orientation of the in-plane hydrogen towards the ring C–H fragment and represents a rotational minimum [12]. The core spectra should not be influenced by the nearly free rotation of the methyl group, as such rotation affects only certain valence shell molecular orbitals (MOs) [1, 12]. Adenine (Fig. 1), like thymine, has no low-lying tautomers [9, 11, 14, 49]. A planar molecular structure of adenine was assumed here, which differs slightly from the "global minimum" structure exhibiting a small out-of-plane bending of the NH_2 hydrogen atoms. In the planar structure one can utilize C_s symmetry, which significantly simplifies both the ADC calculations and the interpretation of the results.

The polarization propagator ADC(2)/CVS and the one-particle Green's function ADC(4)/CVS calculations were performed using the 6-31+G and 6-31G basis sets [50, 51], respectively. These relatively small basis sets had to be chosen mainly because of computational limitations. As demonstrated in our previous study [30], the 6-31G basis sets lack the flexibility for a sufficiently accurate description of core-hole states, leading to a relatively large, if uniform, overestimation (about 2 eV) of the C 1s excitation energies. The oscillator strengths, on the other hand, are quite satisfactorily reproduced at the 6-31G level [30]. This suggests the application of a uniform shift to the theoretical spectra in order to correct for basis set and other errors of our approach [30]. The diffuse functions employed in the present calculations should allow a reasonably good description of some low-lying 1s-to-Rydberg excitations.

The Hartree-Fock data for the ADC(2) polarization propagator computations [52] were generated using the GAMESS (US) program package [53]. The ionization spectra were calculated using the direct ADC(4)/CVS one-particle Green's function code [54] interfaced to the GAMESS (UK) *ab initio* program package [55].

The theoretical spectral envelopes were generated by convoluting the discrete transitions lines (stick spectrum) with Lorentzians of 0.4-0.7 eV FWHM (full width at half maximum). This accounts for effects of spectrometer resolution, unresolved vibrational structure, and natural life times of the core-hole states.

3. Results.

Before presenting the x-ray absorption spectra, we briefly consider the number of empty π^*-orbitals in each molecule on the basis of electron counting arguments.

The strongest spectral maxima can typically be explained by one or more core-to-valence transitions of large oscillator strengths, and transitions to π*-orbitals are usually the strongest. In the thymine aromatic system there are 8 atomic $2p_z$ orbitals associated with the 4 C and 2 N ring atoms and the 2 O atoms, giving rise to 8 molecular π-orbitals, of which 5 are doubly occupied. Here each of the C (ring) and O atoms contributes just one electron to the π-system, whereas the N atoms of the two NH groups contribute two (lone pair) electrons each. Thus there are three unoccupied π-orbitals (π_6*-π_8*) available in thymine. Note that the correct C_s symmetry labeling of these orbitals is 7a", 8a", and 9a", respectively, since there is another occupied orbital of a" symmetry deriving from the methyl carbon (C_9) $2p_z$ atomic orbital.

In adenine the π-system consists of 9 π-orbitals and 10 electrons, giving rise to 4 unoccupied π-orbitals (π_6*-π_9*). In counting the electrons it should be noted that the pyridinic N atoms each contribute just one electron to the π-system, the lone pair orbital here being of σ-type (in-plane). As in thymine, the correct C_s symmetry labeling of the π*-orbitals is 7a"-11a", as the $2p_z$ atomic orbital of the amino nitrogen, N_3, gives rise to an occupied a" molecular orbital.

The thymine and adenine π* orbitals are displayed in Figs. 1b and 1c, respectively. These plots have been generated using the MOLDEN graphic software [56]. In general, the lowest unoccupied π orbitals, having physical significance, are to a certain extent invariant with respect to the choice of the basis set (if less so than the occupied MOs). However, for larger basis sets, especially ones comprising diffuse functions, it is difficult to identify the π* orbital in the manifold of virtual orbitals. The π* orbital plots in Figs. 1b and 1c have been generated using the small 6-31G basis (without diffuse functions). While these orbitals are essentially delocalised over the entire π-system, one clearly can distinguish bonding and anti-bonding characteristics. The thymine π_6* orbital, for example, reveals C_6-C_8 bonding and C_7-C_8 anti-bonding character.

The π* orbital plots allow for a survey of the expected 1s → π* excitations. Supposing that an excited state wave function has a dominant 1s → π* contribution, the intensity is essentially given by the squared modulus of the dipole matrix element $\langle 1s|\hat{z}|\pi^*\rangle$. Due to the localization of the 1s orbital, this matrix element will directly reflect the charge density of the π* orbital at the (atomic) site of the 1s orbital. In

particular, the dipole integral will be small (or vanishing) if the electron density of the π* orbital is small (vanishes) at the site of the 1s orbital due to the lack of overlap. Thus by mere inspection of the π* orbital plots one can sort out low (or zero) intensity transitions. According to Fig. 1b, for example, the thymine π_6* orbital has no (or little) electron density at the C_5 atom, which means that the dipole integral $\langle C_5 1s | z | \pi_6^* \rangle$, and thus the $C_5 \rightarrow \pi_6$* intensity, will be very small. In the same way one can rule out the presence of noticeable $C_9 1s \rightarrow \pi_6$*, $C_9 1s \rightarrow \pi_7$*, $C_7 1s \rightarrow \pi_7$*, and $O_1 1s \rightarrow \pi_6$* transitions in thymine, or $C_8 1s \rightarrow \pi_6$* and $C_7 1s \rightarrow \pi_7$* in adenine.

It should be emphasized that the characterization of the excited states in terms of a single dominant excitation is an oversimplification, as the actual excited states are more adequately represented by linear combinations of several singly excited configurations with substantial admixtures of double (and higher) excitations. But for a qualitative understanding of the spectral features the single excitation (SE) picture is often quite useful. To the extent that the SE picture is applicable, one may say that the 1s → π* excitations probe the local electron density of the π* orbital at the respective (atomic) 1s sites.

3.1. C 1s absorption spectrum of thymine.

In Fig. 2 theoretical and experimental C 1s X-ray absorption spectra of thymine are compared. The ADC(2) excitation energies and oscillator strengths are also given in Table 1 together with the experimental peak positions. Note that the theoretical energies have been shifted by –2.52 eV to achieve optimal overall agreement with the experimental data. The shift represents the mean deviation of the ADC(2) energies relative to the positions of the clearly resolved experimental band maxima.

According to our calculations, the lowest C 1s absorption maxima A and B of thymine at 284.9 and 285.9 eV can be assigned to the transitions C_8 1s → π_6* and C_7 1s → π_6*, respectively. The present calculations show that the high-energy shoulder of the peak B at about 286.5 eV (B') is due to the transitions C_9 1s → π_6* and C_9 1s → 3s, rather than to unresolved vibrational progressions accompanying the transition C_7 1s → π_6* (as might be surmised from the shape of the experimental profile).

The next spectral band is more complex and shows three features C, D, and E at 287.3, 287.8 and 288.4 eV, respectively. In the energy range 287.0-288.5 eV, our calculations predict several transitions of both valence and Rydberg character. As seen from Fig. 2, the shape of the spectral envelope here is formed by the superposition of all these transitions. In particular, the C_8 1s → π_7* valence and C_9 1s → 3p Rydberg transitions contribute to the shoulder C. The maximum D originates mainly from the excitations C_6 1s → π_6*, C_9 1s → π_8* and Rydberg excitation, C_9 1s → 3p. The shoulder E is formed solely of Rydberg transitions, C_9 1s → 4s and C_7 1s → 3s, having quite appreciable oscillator strength.

The most prominent absorption band F with its maximum at 289.4 eV is in the spectral interval 289.2-290.2 eV. According to our calculations this band derives its intensity mainly from the valence transition C_5 1s → π_7*, but also many other low-intensity transitions contribute in this interval. The dense spectral structure of mixed valence and Rydberg character can be seen at the low-energy side of the band F (Table 1). In our calculations these transitions give rise to a shoulder seen in the theoretical spectrum at about 289 eV, which however has no obvious counterpart in the experimental curve.

The calculations of the spectral region near the ionization threshold show minor disagreement with the experimental data. The main spectral feature here is the maximum G at 290.7 eV, which is reproduced by the present calculations as a high-energy shoulder of the band F at about 290.3 eV. The largest contribution to the intensity of the band G is the valence transition C_8 1s → π_8*, but also the neighboring Rydberg transitions such as C_9 1s → 5p and C_9 1s → 5s have quite significant oscillator strengths.

3.2. N 1s absorption spectrum of thymine.

In figure 3, we compare the experimental and theoretical spectra at the nitrogen edge, with the theoretical values shifted by –2.59 eV, similar to the shift for carbon. Our calculations show the N 1s X-ray absorption spectrum of thymine is characterized by a dense group of transitions with a rather complex pattern even at the lowest energy. The calculations reproduce the N 1s absorption envelope less accurately than in the case of the C 1s spectrum, which can be expected from the increased complexity of the N 1s excitation manifold. The main difference between the

theoretical and experimental spectra is that the distinct experimental bands A and B with maxima at 401.7 and 402.7 eV merge in the theoretical spectrum into a single band. Band A is assigned to transitions N_4 1s → π_6*, N_3 1s → π_6* and N_3 1s → 3s, while band B comprises transitions N_4 1s → 3s, $N_{4,3}$ 1s → π_7* and N_4 1s → 3p (Table 2). Interestingly, all these transitions are characterized by high relative oscillator strengths ranging from 0.3 to 1.0.

The spectral band C with maximum at 404.1 eV is well reproduced by our calculations, and according to the present theoretical results originates from a group of mainly Rydberg transitions in the 403.8-404.1 eV interval. We tentatively assign the transitions 5^1A" or 6^1A" of this group to valence or mixed valence-Rydberg type (N_4 1s → π_7*/3p and N_3 1s → 3p/π_7*, respectively).

The next part of the experimental N 1s spectrum of thymine is characterized by an increase of the photoabsorption intensity above 404.6 eV that approaches maximum (D) at 405.5 eV, just below the N 1s ionization threshold. According to our calculations, several Rydberg and valence transitions contribute to this part of the spectrum. The most prominent transitions, being of direct relevance for the maximum D are $N_{4,3}$ 1s → 5s, $N_{4,3}$ 1s → 5p and N_3 1s → π_8*. A very strong N_4 1s → π_8* transition (f = 0.97), is predicted at about 0.5 eV in the (first) N 1s ionization continuum.

3.3. O 1s absorption spectrum of thymine.

Figure 4 displays the experimental and theoretical spectra of thymine at the oxygen edge, with the theoretical data displaced by –2.19 eV to optimally match the experimental data. This shift is close to the shifts applied at the C and N edges. The O 1s absorption spectrum of thymine can be subdivided into two distinct parts: the low-energy part consists of the two intense maxima A and B at 531.4 and 532.3 eV, respectively. According to the present theoretical results, the peaks A and B with nearly equal intensity are due to the valence transitions O_2 1s → π_6* and O_1 1s → π_7*, respectively (Table 3). The orbital plots in Fig. 1b are consistent with the presence of the latter two transitions and also explain the absence of a discernible O_1 1s → π_6* transition.

According to the π_7* orbital plot one would also expect a distinct O_2 1s → π_7* transition of similar strength as that of O_1 1s → π_7*. Apparently, however, a

corresponding feature is missing both in the experimental spectrum and the computational results. In the energy region above 534 eV one finds the onset of O 1s → ns,np Rydberg excitations, and, moreover, a strong mixing the O_2 1s → π_7* configuration with the lowest members of the np Rydberg series. This means there is π_7* (and π_8*) character in the higher energy part of the spectrum, not being focused in a single transition but rather spread out over several final states of relatively small spectral strengths due to the strong mixing with Rydberg excitations. Obviously, here the picture of a dominant single excitations fails, and the simple overlap criterion for the intensities no longer applies.

In agreement with the experimental spectral profile, our theoretical results predict more specifically two groups of transitions contributing to bands C and D, respectively. Transitions contributing to the band C are located within the 535.1-536.1 eV interval. These are various 3p and 4p Rydberg transitions with substantial contributions of π_7*-character. The band D in the 536.7-537.2 eV interval encompasses transitions of the 4s and 4p type with of π_8* contributions (Table 3).

3.4. C 1s, N 1s and O 1s photoelectron spectra of thymine.

The experimental and theoretical C 1s, N 1s, and O 1s photoionization spectra of thymine are shown in Figs. 5-7 and the numerical data is listed in Table 4.

The C 1s XPS spectrum of thymine in Fig. 5 shows four distinct peaks A-D at 291.0, 292.3, 294.2 and 295.2 eV, respectively, which are rather well reproduced by the present calculations. According to our results the energetically lowest band comprises two close-lying ionic states, $(C_8\ 1s)^{-1}$ and $(C_9\ 1s)^{-1}$, separated by only 0.28 eV (Table 4). Interestingly, at the HF level (Table 4) the order of these states is reversed, the $(C_9\ 1s)^{-1}$ state lying about 0.9 eV below its counterpart. This reversal of the HF chemical shift ordering (see Sec. 4.1) is caused by a non-uniform relaxation effect. The relaxation energy associated with the creation of a C 1s vacancy in the methyl group (13.1 eV) is distinctly smaller than the C 1s relaxation energy for the C_8 ring atom (14.2 eV). It should be noted that the difference in the relaxation energies is also reflected by the different spectroscopic factors 0.64 and 0.57. The remaining three peaks in the experimental spectrum, assigned to the ionic states $(C_7\ 1s)^{-1}$, $(C_6\ 1s)^{-1}$ and $(C_5\ 1s)^{-1}$, respectively, are in good agreement with the chemical shifts at

the HF level. Our calculations also predict that several low-lying 2h-1p satellites with rather low intensities contribute to peak D.

The N 1s and O 1s ionization spectra of thymine are particularly simple (Figs. 6 and 7). In each case there are two non-equivalent nitrogen or oxygen atoms, exhibiting only minor chemical shifts. Accordingly, our ADC(4) calculations yield close-lying pairs of N 1s and O 1s ionic states with energy splittings of 0.28 and 0.22 eV, respectively. The convoluted spectral profiles for these N 1s and O1s pairs fit quite nicely to the broad unresolved experimental peaks (A) in Figs. 6 and 7, respectively.

The gas phase core emission spectra of thymine have also been calculated by Takahata et al [3]. We obtain the same order of binding energies but rather better agreement for energy differences between the C 1s peaks, particularly for the two highest binding energy peaks. For nitrogen and oxygen, we agree that the two core levels should appear as an unresolved single peak.

3.5. C 1s absorption spectrum of adenine.

The results for the X-ray absorption of adenine are presented in Figs. 8 and 9 and Tables 5 and 6. The spectrum is not flat at lowest energies due to difficulties in normalizing the intensity at this energy. Here the shifts applied to the calculated C 1s, and N 1s spectra are –2.59 and –2.39 eV, respectively.

The photoabsorption of adenine in the 286-288 eV energy range manifests itself by a complex band structure with the maxima A-C near 286.4, 286.8 and 287.4 eV, respectively, and shoulders A' and C' near 286.0 and 288.0 eV, respectively (Fig. 8). The calculations show that this part of the spectrum is formed by at least eight transitions most of which have valence character (Table 5). The present calculations reproduce correctly the positions of the peaks in the experimental spectrum, but predict less accurately their relative intensities: for example, the calculated relative intensities of the maxima A and B are just the opposite of the experimental results.

According to our calculations the lowest transition in the spectrum C_{10} 1s $\rightarrow \pi_6^*$ at 286.07 eV is not very intense ($f = 0.199$). Consequently, it does not lead to a separate peak in the spectral envelope, but rather to a low-energy shoulder A' of band A. The next two transitions C_{10} 1s $\rightarrow \pi_7^*$ and C_9 1s $\rightarrow \pi_{6,7}^*$ come virtually on top of each other at about 286.4 eV and give rise to peak A. It should be noted that the

oscillator strength of the latter transition, being more adequately described as a superposition of C_9 1s → π_6* and C_9 1s → π_7*, is nearly 3.5 times higher than that of the former. According to our results peak B is due to the single transition C_7 1s → π_6* with rather high *f* value of 0.877. The peak C is formed by the two intense valence transitions C_6 1s → π_6* and C_8 1s → π_7* (*f* = 1.000 and 0.972, respectively) and by a weak Rydberg transition C_{10} 1s → 3s (*f* = 0.004). The high-energy shoulder C' originates according to the present theoretical results from the valence transition C_{10} 1s → π_9*.

The part of the NEXAFS adenine spectrum above 288 eV does not show well resolved bands or pronounced peaks. Instead, one observes a steady increase of the absorption cross section towards the ionization threshold. The barely visible maxima D-G in this region are due to many low-intensity transitions of Rydberg and valence nature (Table 5), and their accurate assignment is difficult. The tentative assignments proposed in Fig. 8 are shown as an example of how the groups of the calculated transitions can be related to the experimental results.

Moewes et al [6] have reported in graphical form the calculated C 1s spectrum. While they correctly predict peaks B and C, peaks A and A' are missing from their calculation, so our results represent a considerable improvement.

3.6. N 1s absorption spectrum of adenine.

The N 1s NEXAFS spectrum of adenine (Fig. 9) is characterized by three prominent bands A-C below the N 1s ionization limit. The lowest band A with a maximum near 399.5 eV has complex spectral structure and consists of the three major valence transitions, N_4 1s → π_6*, N_2 1s → π_6*, and N_5 1s → π_7* accommodated within a narrow energy interval of only 0.4 eV (Table 6). Having significant *f* values, the superposition of these three transitions leads to a very intense peak in the overall spectral envelope. In view of the limited accuracy of the ADC(2) method the computed order of the transitions composing band A has to be taken with a grain of salt.

Our calculations predict a weak valence transition N_4 1s → π_7* (*f* = 0.082) at 400.69 eV, which correlates with the structure A' of the experimental spectrum at about 400.4 eV that appears to be a poorly resolved shoulder of the band A.

The next two bands B and C of the experimental spectrum with maxima near 401.9 and 403.0 eV are not so well reproduced by our calculations. In the calculated spectrum, the two bands merge into a single band, which does not allow a clear cut interpretation of the experimental results. However, some assignments are possible, for example, it is reasonable to assign the calculated transitions to the bands B and C, as proposed in Fig. 9.

The spectral structure seen on the low-energy side of the band B near 401.0-401.3 eV and denoted as the shoulder B' correlates with a group of absorption lines predicted by our calculations in the 401.4-401.6 eV interval. These are mainly 3s Rydberg excitations from the 1s orbitals of the N_2, N_3, N_4 and N_5 atoms. The strongest transition in the group is the valence excitation N_3 1s $\rightarrow \pi_{6,7}^*$ with the oscillator strength $f = 0.303$.

The main source of the photoabsorption intensity of the experimental band B according to our calculations are valence transitions N_1 1s $\rightarrow \pi_{6,7}^*$ ($f = 0.629$) and N_2 1s $\rightarrow \pi_7^*$ ($f = 0.121$) at 402.07 and 402.0 eV, respectively. The rest of the transitions in the energy range of the experimental band B (402.0-402.7 eV) are various Rydberg (3p, 3s and 4s) transitions from different N 1s orbitals (Table 6).

Our calculations predict that the band C (402.8-403.5 eV) is mainly composed of Rydberg transitions, principally to 4p states from different N 1s orbitals. Interestingly, the predicted spectral intensities of the three valence transitions N_2 1s $\rightarrow \pi_8^*$ N_4 1s $\rightarrow \pi_8^*$ and N_1 1s $\rightarrow \pi_7^*$, also falling in the same energy interval, are insignificant compared to the large oscillator strength ($f = 0.480$) of the Rydberg transition N_3 1s $\rightarrow$ 4p, which dominates the photoabsorption associated with the band C.

Above 403.5 eV the photoabsorption cross section of adenine increases evenly toward the N 1s ionization threshold (~ 404.4 eV). Our calculations predict in this energy range higher members of various Rydberg series and some higher-lying valence transitions (Table 6).

3.7. C 1s and N 1s photoelectron spectra of adenine.

The C 1s XPS spectrum of adenine in Fig. 10 consists of two bands A and B with maxima near 291.0 and 292.5 eV, respectively; the data is summarized in Table 7. We attribute the lowest band A to the $(C_{10}\ 1s)^{-1}$ ionization, and the energetically

higher band B to the $(C_9\ 1s)^{-1}$, $(C_8\ 1s)^{-1}$, $(C_7\ 1s)^{-1}$ and $(C_6\ 1s)^{-1}$ ionic states. Apparently, our calculations slightly overestimate the splitting between the $(C_9\ 1s)^{-1}$ and $(C_8\ 1s)^{-1}$ states, giving rise to a distinct maximum at the low-energy flank of the B profile, which is however not visible in the experimental curve.

The N 1s XPS spectrum of adenine (Fig. 11) shows three distinct peaks A-C with maxima at 404.4, 405.7 and 406.7 eV, respectively. According to our calculations the low-energy band A is due to the $(N_5\ 1s)^{-1}$, $(N_4\ 1s)^{-1}$ and $(N_2\ 1s)^{-1}$ ionic states. As for thymine, the computed splitting of the $(N_4\ 1s)^{-1}$ and $(N_2\ 1s)^{-1}$ states is somewhat too large, leading to an additional maximum in the theoretical spectrum at 404.99 eV. Peak B is exclusively due to ionization from the amino group nitrogen, $(N_3\ 1s)^{-1}$. At the HF level (Table 7), the N 1s binding energies of the sites 2-5 are very similar, and the energy spread of the final N 1s ionic states is essentially due to relaxation. In particular, the distinctly different ionization energy of the $(N_3\ 1s)^{-1}$ ionic state is due to the smaller relaxation energy (16.9 eV) of the amino group nitrogen as compared to the relaxation energies of the N 1s sites in the aromatic system (17.6-17.9 eV). The high-energy peak C at 406.7 eV is again solely due to the $(N_1\ 1s)^{-1}$ ionic state. The relatively strong chemical shift of this NH group nitrogen is discussed below.

Takahata et al [3] have also calculated the core photoemission spectra of adenine. For C 1s our calculations agree better with experiment for the separation between the smaller peak A and the unresolved group of peaks B, although we do not predict exactly the shape of peak B. We agree on the order of the ionization potentials, although we note that C_7 and C_8 have energies that are very close together, 190 meV in our calculation, 20 meV in that of Takahata et al. For nitrogen we agree on the order of the ionization potentials, and obtain improved agreement for their energy differences.

4. Discussion

4.1. Chemical shifts in the photoelectron spectra of thymine and adenine.

While the magnitude of the K-shell excitation energies is given by the respective atomic 1s electron binding energies, being about 290, 400, and 540 eV for C, N, and O, respectively, there are considerable “chemical shifts” [57] in the 1s

electron binding energies for non-equivalent sites of the same element in a molecule. In thymine, for example, there are five non-equivalent C atoms, leading to energy differences in the C 1s energies of up to 5 eV. It is well known that these chemical shifts can largely be rationalized by screening (charge supply) or anti-screening (charge withdrawal) effects induced by the neighbouring atoms, i.e. by relative electronegativities. Screening leads to a lowering of the 1s binding energy, whereas anti-screening causes an increase. While the chemical shifts are manifest in the core-level ionization spectra, their impact, if somewhat diminished, will also be seen in the core-level excitation spectra.

The chemical shifts reflect the charge distribution in the neutral molecule and, thus, can be inspected at the level of the HF orbital energies ($-\varepsilon_{1s}$). Let us consider the C 1s orbital energies of thymine, as given in Table 4. The lowest C 1s binding energy (304.0 eV) pertains to the carbon (C_9) of the methyl group. (Note that the atoms in Fig. 1 are numbered according to decreasing 1s binding energies.) The lowest C 1s binding energy of the ring atoms, 304.9 eV, is associated with the C_8 atom, which has three C atoms as immediate neighbours. Carbon atom C_7 is neighbouring with the more electronegative N atom, which leads to an increase of the 1s binding energy of almost 2 eV with respect to C_8 (306.7 eV). The largest 1s binding energies, 308.3 and 309.4 eV, are found for the two C atoms of the carbonyl groups, C_5 and C_6, respectively. The larger binding energy of C_5 is due to the fact that C_5, in addition to the oxygen, has two N neighbours, whereas C_6 has only one. The N 1s binding energies of the N_3 and N_4 atoms differ only slightly (0.3 eV), and the separation between the O 1s energies of O_1 and O_2 is even smaller (0.1 eV).

The relative C 1s binding energies of the 5 non-equivalent C atoms in adenine can be rationalized in a similar way (see Table 7). There is one C atom (C_{10}) with only one N neighbour (binding energy 305.1 eV), whereas the remaining C atoms have two neighbouring nitrogen atoms each, with binding energies ranging from 306.5 eV (C_9) to 307.4 eV (C_6). The N 1s binding energies of the N_3 (amino-group) and pyridinic nitrogens (N_2, N_4, N_5) are very similar (422.0-422.6 eV), but there is a distinctly larger N 1s binding energy (424.0 eV) for the NH group nitrogen (N_1). A tentative explanation for the enhanced 1s binding energy of the NH nitrogen is as follows. In contrast to a pyridinic nitrogen, which has an (in-plane) σ-type lone-pair orbital and contributes one electron to the π-system, the lone-pair orbital of the NH nitrogen is

part of the π-system, to which it commits two electrons altogether. The (partial) delocalization of these electrons results in a net charge loss of the NH group nitrogen, compared to the pyridinic N atom.

4.2 Relaxation effects in the photoelectron spectra of thymine and adenine.

The comparison between the HF and ADC(4) ionization energies in Tables 4 and 7 allows one to assess the role of the relaxation effect, that is, the rearrangement of the outer-shell (valence) electrons in response to the removal of a core-level electron. This relaxation effect leads to a considerable energy lowering of the final ionic state compared to the HF result corresponding to a "frozen" initial charge distribution. To a first approximation, the relaxation energy is specific to the respective atom, being in the order of 12, 15, and 18 eV for the C, N, and O atoms, respectively. But there is also an additional contribution associated with the embedding molecular environment. Whereas the C 1s relaxation energy of the methyl group carbon (13.1 eV) is only slightly larger than the atomic value, there is a distinctly larger relaxation effect for the "aromatic" carbon atoms, amounting to about 14.1 eV (mean value) for the thymine molecule and to 14.5 eV for the larger aromatic system of adenine.

The size of the relaxation effect (relative to 1s ionization of the same atomic species) is also reflected by the spectroscopic factors, P_n, being a measure for the relative spectral strengths of the final ionic states $\left|\Psi_n^{N-1}\right\rangle$. The P_n values for the C 1s hole states associated with the aromatic C atoms are about 0.58 for thymine and even somewhat smaller for adenine (mean value 0.55). A similar picture is seen for the N 1s hole states, where the P_n values are 0.58 for thymine and 0.54 for adenine (mean value for the nitrogen atoms in the aromatic system). Still smaller P_n values (0.51) are found for the O 1s hole states in thymine. This means that more than 40% and up to 50% of the spectral strength is diverted from the 1s single-hole states towards "shake-up" satellites, and strong two-hole-one-particle satellites of the $1s^{-1}\pi^{-1}$-π* type have to be expected at higher energies in the C 1s, N 1s, and O 1s ionization spectra.

4.3 Absolute energy accuracy of the calculations

The fourth-order ADC(4) method used in calculations of the ionization energies is more accurate than the ADC(2) approach to the core-level excitation, still there is a

uniform error in the order of 1-2 eV in the calculated XPS spectra. This disagreement is essentially due to the insufficiency of the 6-31G basis set used here. As in the excitation spectra, the ADC(4) results have been adjusted by uniform shifts of −1.9, −2.2 and −1.2 eV for the thymine C 1s, N 1s, and O 1s spectra, respectively, and −1.61 and −1.62 eV for the adenine C 1s and N 1s spectra, respectively.

4.4 Rydberg excitations and π resonances*

With regard to the NEXAFS spectra, Rydberg excitations appear to be quite important for the K-shell photoabsorption spectra of both molecules. The Rydberg structure has an onset at rather low excitation energies and extends towards the ionization limits. It should be noted, however, that in the case of the carbonylic C_5 and C_6atoms in thymine, the $C_{6,5}$ 1s → Rydberg transitions set in only at a rather large energy, possibly already above the C_8 ionization threshold at 291 eV. Many of the core-to-Rydberg transitions have appreciable oscillator strengths, and since they overlap the core-to-valence excitations, the distinction of valence and Rydberg transitions in the present spectra is often not clear cut. Moreover, many transitions of thymine and adenine have, in fact, mixed Rydberg-valence character.

Whereas part of the formally possible 1s → π* excitations does not appear in the excitation spectrum due to the lack of intensity, as discussed at the beginning of Sec. 3, other excitations, sufficiently equipped with spectral strength, will be missing in the discrete part of the spectrum because their excitation energies exceed the (lowest) 1s ionisation threshold, which makes them 1s → π* resonances in the 1s ionisation continuum. This concerns primarily excitations involving the energetically highest π* orbitals, that is, π_8* in thymine, and π_9* in adenine with orbital energies of 7.7 and 10.1 eV, respectively. Assuming a dominant 1s-π* single excitation, the excitation energy can be assessed from the first-order expression $\varepsilon_{\pi^*} - \varepsilon_{1s} - J_{1s,\pi^*}$ where J_{1s,π^*} is the Coulomb integral associated with the interaction of the 1s and π* charge distributions. It should be borne in mind, however, that second-order contributions, i.e. relaxation (response to the removal of a 1s electron) and polarization (response to the promotion of an electron into the π* orbital), are substantial. (For the term values, $\tau_n = \Omega_n - IP_{1s}$, the relaxation contributions cancel,

so that the first-order term value, $\varepsilon_{\pi^*} - J_{1s,\pi^*}$, has to be augmented only by the polarization contribution.) The (positive definite) J_{1s,π^*} Coulomb integral becomes large if the 1s core and the π* orbital have a region of non-vanishing overlap, that is, if the π* orbital has noticeable charge density at the 1s site. A local π* orbital charge at the 1s site means an excitation induced screening effect for the 1s core hole, resulting in a lowering of the excitation energy. The larger the local π* orbital charge, to be assessed by inspection of the orbital plot, the lower the corresponding 1s → π* excitation energy. As an example, let us consider the $C_8$1s → π_6* and $C_8$1s → π_7* excitations in adenine. As seen in the orbital plots in Fig. 1c, the charge density at the C_8 atom is small for π_6* and large for π_7*. Accordingly, the $C_8$1s → π_7* transition has a smaller excitation energy (287.5 eV) than the (low-intensity) $C_8$1s → π_6* transition (288.0 eV) despite the energy difference of the π_6* and π_7* orbital energies (1.9 eV).

4.5. Comparison with condensed phase data. As mentioned above, Moewes et al [6] have reported the C edge NEXAFS spectra of thymine and adenine, and accompanying calculations. Samuel et al. [58] have also reported NEXAFS spectra of all edges of thymine and adenine in the condensed state. For the thymine C edge, the overall x-ray spectral structure is preserved in the transition from the gaseous to the condensed phase. Our peaks A, B, D and F can be associated with peaks 1, 2, 3 and 4 of Moewes et al, and the corresponding peaks of Samuel et al. The spectra are broader in the solid state, as usual; our data show more detail and allow a more precise assignment. Samuel et al assigned the peaks A, B, D, and F according to our designation to transitions labelled as $\pi^*_{C=C}$, $\pi^*_{C=C-N}$, π^*_{CONH}, π^*_{HNCONH}, respectively. Here the respective C 1s orbitals are designated somewhat indirectly by the subscript chemical shift patterns, which readily translate according to C=C (C_8), C=C-N (C_7), CONH (C_6), and HNCONH (C_5) into our numbering scheme. If the subscripts are not meant to characterize the respective π* orbitals as well, the assignment of Samuel et al. agrees with that of ours. It should, however, be recalled that the π_6* orbital is involved in the first three transitions (A, B, D) and π_7* in the transition D. Both π* orbitals, spreading out over the entire π-system, show C_6=O_2 anti-bonding character; strong C_5=O_1 anti-bonding character is present in the π_7* orbital.

For adenine the shapes of the C edge NEXAFS spectra in the solid state are similar, but there is an additional peak at 285.1 eV [58], which is not present in our results. We associate the solid state peaks at 286.5 and 287.5 with our features A+B (average energy 286.6) and C (287.4 eV) respectively. Samuel et al assigned their first features to $\pi^*_{C=C}$, the other two without further specification to π^*_{C-Nx} species. However adenine does not contain a functional group corresponding to $\pi^*_{C=C}$, that is, two carbon atoms, of which neither is bonded to a nitrogen atom. All carbon atoms are bonded to one or two N atoms. Thus the 285.1 eV peak seems to be a feature of the solid state.

The nitrogen K edge NEXAFS spectra of condensed thymine and adenine [58] appear to be broadened versions of the gas phase spectra. As we have shown, these are rather complicated manifolds of states. At the oxygen edge the splitting of the strong π^* states (531.4, 532.3 eV) is still visible in the solid (531.8, 533.0 eV) – we have assigned these two transitions.

X-ray absorption and photoemission spectra have also been measured by Furukawa et al [59] at the nitrogen and oxygen edges of thymine adsorbed on Cu(110). At the nitrogen K edge, our features A, B and D appear to correspond to the features A_2, A_2" and B_2, where the peaks are shifted by about 2.3 eV to lower energy in the condensed phase. Assuming the photon energy was well calibrated, this is a rather strong chemical shift for a NEXAFS spectrum. From our calculations, peak A_2 is assigned to N_4 1s $\rightarrow \pi_6^*$, N_3 1s $\rightarrow \pi_6^*$, 3s transitions, while peak A_2" is assigned to N_4 and N_3 1s $\rightarrow \pi_7^*$/3p transitions. This information resolves an anomaly in the interpretation of the spectra of Furukawa et al: all peaks were assigned generically to π^* resonances, and so should show the same polarization dependence. However in some geometries, the peaks A_2 and A_2" appear with different intensity ratios. This may be because the resonances do not have pure π^* character, but are the sum of several resonances.

The oxygen K edge NEXAFS spectrum of Furukawa et al is similar to our gas phase spectrum, but shifted by about 0.5 eV to higher photon energy. We assign their resonances X_2 and X_2' from our calculations to O_2 1s $\rightarrow \pi_6^*$ and O_1 1s $\rightarrow \pi_7^*$ respectively.

The O 1s photoemission spectra of adsorbed thymine show a single peak, as in the gas phase, but shifted by 6.2 eV, most likely due to screening effects. The nitrogen spectrum shows two peaks, compared with a single peak in the gas phase, shifted by 5.5 and 7.2 eV respectively. The first peak has undergone a screening shift, while the second has undergone an additional chemical shift. This supports the interpretation of these authors [59] that bonding to the surface occurs through the nitrogen atom located between the two oxygen atoms.

5. Conclusions.

The core level photoabsorption and photoemission spectra of two nucleobases, thymine and adenine, have been measured at the C, N and O 1s edges and interpreted with the aid of polarization propagator ADC(2) and one-particle Green's function ADC(4) calculations. The photoemission spectra are in very good agreement with theory for all core levels, and the spectra have been assigned in detail. The overall agreement between theory and experiment is very good for the NEXAFS spectra at the O and C edges of thymine and the C edge of adenine. There are some discrepancies for the N edges of both molecules, but the overall spectral shape can be explained.

Acknowledgements.

It is a great pleasure to dedicate this paper to Wolfgang Domcke on the occasion of his 60th birthday. Having been the third mate on the climbing rope, figuratively speaking, J. Schirmer is indebted to Wolfgang for inspiration, education, and encouragement in the “early” years.

The theoretical part of this study was supported by grants of the Russian Foundation for Basic Research (RFBR) and the Deutsche Forschungsgemeinschaft (DFG). We gratefully acknowledge the assistance of our colleagues at Elettra for providing good quality synchrotron light.

O. Plekan acknowledges financial support from the Area di Ricerca di Trieste under the Incoming Mobility scheme. V. Feyer thanks the Abdus Salaam International Center for Theoretical Physics for a TRIL (Training and Research in Italian Laboratories) fellowship. E. V. Gromov wishes to thank H. Köppel and L. Cederbaum for helpful discussions.

References.

[1] A. B. Trofimov, J. Schirmer, V. B. Kobychev, A. W. Potts, D. M. P. Holland, and L. Karlsson, J. Phys. B: At. Mol. Opt. Phys. 39 (2006) 305.

[2] R. S. Brown, A. Tse, and J. C. Vederas, J. Am. Chem. Soc. 102 (1980) 1174.

[3] Y. Takahata, A. K. Okamoto, and D. P. Chong, Int. J. Quantum Chem. 106 (2006) 2581.

[4] Y. Mochizuki, H. Koide, T. Imamura and H. Takemiya, J. Synchrotron Rad. 8 (2001) 1003.

[5] H. Ågren, V. Carravetta, O. Vahtras, and L.G.M. Pettersson, Chem. Phys. Lett. 222 (1994) 75;
H. Ågren, V. Carravetta, O. Vahtras, and L. G. M. Pettersson. Theor. Chem. Acc. 97 (1997) 14.

[6] A. Moewes, J. MacNaughton, R. Wilks, J. S. Lee, S. D. Wettig, H.-B. Kraatz, E. Z. Kurmaev, J. Electron Spectrosc. Relat. Phenom. 817 (2004) 137.

[7] M. Y. Choi and R. E. Miller, J. Phys. Chem. A 111 (2007) 2475.

[8] P. Colarusso, KeQing Zhang, Bujing Guo, P. F. Bernath, Chem. Phys. Lett. 269 (1997) 39.

[9] C. Fonseca Guerra, F. M. Bickelhaupt, S. Saha and F. Wang, J. Phys. Chem. 110 (2006) 4012.[10] M. J. Scanlan and I. H. Hillier, J. Am. Chem. Soc. 106 (1984) 3737.

[11] O. Dolgounitcheva, V. G. Zakrzewski, and J. V. Ortiz, Int. J. Quantum Chem. 80 (2000) 831.

[12] O. Dolgounitcheva, V. G. Zakrzewski, and J. V. Ortiz, J. Phys. Chem. A 106 (2002) 8411.

[13] J. Rejnek, M. Hanus, M. Kabeláč, F. Ryjáček, and P. Hobza, Phys. Chem. Chem. Phys. 7 (2005) 2006.

[14] M. Hanus, M. Kabeláč, J. Rejnek, F. Ryjáček, and P. Hobza, J. Phys. Chem. B 108 (2004) 2087.

[15] Y. Huang and H. Kenttämaa, J. Phys. Chem. A 107 (2003) 4893.

[16] T. Zeegers-Huyskens, A. K. Chandra, and M. T. Nguyen, J. Phys. Chem. A, 108 (2004) 1101.

[17] O. Plekan, R. Richter, V. Feyer, M. Coreno, M. De Simone, K. C. Prince, Chem. Phys. 334 (2007) 53.

[18] K. C. Prince, R. R. Blyth, R. Delaunay, M. Zitnik, J. Krempasky, J. Slezak, R. Camilloni, L. Avaldi, M. Coreno, G. Stefani, C. Furlani, M. de Simone, S. Stranges, J. Sync. Rad. 5 (1998) 565.

[19] T. D. Thomas, R. W. Shaw, Jr., J. Electron Spectroscopy Relat. Phenom. 5 (1974) 1081.

[20] V. Myrseth, J.D. Bozek, E. Kukk, L.J. Sæthre, and T.D. Thomas, J. Electron Spectroscopy and Relat. Phenom. 122 (2002) 57.

[21] J. Schirmer, Phys. Rev. A 26 (1982) 2395.

[22] A. B. Trofimov, J. Schirmer, J. Phys. B: At. Mol. Phys. 28 (1995) 2299.

[23] L. S. Cederbaum, W. Domcke, J. Schirmer, Phys. Rev. A 22 (1980) 206.

[24] A. Barth, J. Schirmer, J. Phys. B: At. Mol. Phys. 18 (1985) 867.

[25] J. Schirmer, A. Barth, F. Tarantelli, Chem. Phys. 122 (1988) 9.

[26] J. Schirmer, A. B. Trofimov, K. J. Randall, J. Feldhaus, A. M. Bradshaw, Y. Ma, C.T. Chen, F. Sette, Phys. Rev. A 47 (1993) 1136.

[27] H. Köppel, F. X. Gadea, G. Klatt, J. Schirmer, and L. S. Cederbaum, J. Chem. Phys. 106 (1997) 4415.

[28] A. B. Trofimov, T. E. Moskovskaya, E. V. Gromov, N. M. Vitkovskaya, J. Schirmer, J. Struct. Chem. 41 (2000) 483.

[29] A. B. Trofimov, T. E. Moskovskaya, E. V. Gromov, H. Köppel, J. Schirmer, Phys. Rev. A 64 (2001) 022504.

[30] I. Bâldea, B. Schimmelpfennig, M. Plaschke, J. Rothe, J. Schirmer, A. B. Trofimov, Th. Fanghänel, J. Electron Spectrosc. Relat. Phenom. 154 (2007) 109.

[31] V. Carravetta, H. Ågren, L.G.M. Pettersson, O. Vahtras, J. Chem. Phys. 102 (1995) 5589.

[32] L. Triguero, L.G.M. Pettersson, H. Ågren, Phys. Rev. B 58 (1998) 8097.

[33] H. Oji, R. Mitsumoto, E. Ito, Y. Ouchi, K. Seki, T. Yokoyama, T. Ohta, N. Kosugi, J. Chem. Phys. 109 (1998) 10409.

[34] C. Kolczewski, R. Püttner, O. Plashkevych, H. Ågren, V. Staemmler, M. Martins, G. Snell, A.S. Schlachter, M. Sant'Anna, G. Kaindl, L.G.M. Pettersson, J. Chem. Phys. 115 (2001) 6426.

[35] J.C. Slater, Adv. Quant. Chem. 6 (1972) 1.

[36] O. Goscinski, B.T. Pickup, G. Purvis, Chem. Phys. Lett. 22 (1973) 167.

[37] J. Schirmer, L. S. Cederbaum, O. Walter, Phys. Rev. A. 28 (1983) 1237.

[38] W. von Niessen, J. Schirmer, L. S. Cederbaum, Comp. Phys. Rep. 1 (1984) 57.

[39] J. Schirmer, G. Angonoa, J. Chem. Phys. 91 (1989) 1754.

[40] G. Angonoa, O. Walter, J. Schirmer, J. Chem. Phys. 87 (1987) 6789.

[41] J. Schirmer, A. Thiel, J. Chem. Phys. 115 (2001) 10621.

[42] A. Thiel, J. Schirmer, H. Köppel, J. Chem. Phys. 119 (2003) 2088.

[43] N. V. Dobrodey, A. I. Streltsov, L. S. Cederbaum, C. Villani and F. Tarantelli, J. Chem. Phys. 117 (2002) 3533. N. V. Dobrodey, A. I. Streltsov and L. S. Cederbaum, Phys. Rev. A 65 (2002), 22501. N. V. Dobrodey, A. I. Streltsov, L. S. Cederbaum, C. Villani and F. Tarantelli, Phys. Rev. B 66 (2002) 165103. N. V. Dobrodey, L. S. Cederbaum and F. Tarantelli, Phys. Rev. B 61 (2000) 7336.

[44] F. Mertins and J. Schirmer, Phys. Rev. A 53 (1996) 2140.

[45] J. Schirmer and F. Mertins, Int. J. Quant. Chem. 58 (1996) 329.

[46] A. D. Becke, J. Chem. Phys. 98, 5648 (1993); C. Lee, W. Yang, and R. G. Parr, Phys. Rev. B 37 (1988) 758.

[47] R. Krishnan, J. S. Binkley, R. Seeger, and J. A. Pople, Chem. Phys. 72 (1980) 650.

[48] Gaussian 98, Revision A.7, M. J. Frisch, G. W. Trucks, H. B. Schlegel, G. E. Scuseria, M. A. Robb, J. R. Cheeseman, V. G. Zakrzewski, J. A. Montgomery, Jr., R. E. Stratmann, J. C. Burant, S. Dapprich, J. M. Millam, A. D. Daniels, K. N. Kudin, M. C. Strain, O. Farkas, J. Tomasi, V. Barone, M. Cossi, R. Cammi, B. Mennucci, C. Pomelli, C. Adamo, S. Clifford, J. Ochterski, G. A. Petersson, P. Y. Ayala, Q. Cui, K. Morokuma, D. K. Malick, A. D. Rabuck, K. Raghavachari, J. B. Foresman, J. Cioslowski, J. V. Ortiz, A. G. Baboul, B. B. Stefanov, G. Liu, A. Liashenko, P. Piskorz, I. Komaromi, R. Gomperts, R. L. Martin, D. J. Fox, T. Keith, M. A. Al-Laham, C. Y. Peng, A. Nanayakkara, C. Gonzalez, M. Challacombe, P. M. W. Gill, B. Johnson, W. Chen, M. W. Wong, J. L. Andres, C. Gonzalez, M. Head-Gordon, E. S. Replogle, and J. A. Pople, Gaussian, Inc., Pittsburgh PA, 1998.

[49] J. Leszczynski, in The Encyclopedia of Computational Chemistry, John Wiley and Sons: New York, 1998, Vol. 5, p 2951.

[50] W. J. Hehre, R. Ditchfield, and J. A. Pople, J. Chem. Phys. 56 (1972) 2257.

[51] T. Clark, J. Chandrasekhar, and P. v. R. Schleyer, J. Comput. Chem. 4 (1983) 294.

[52] Polarization propagator ADC code written by A. B. Trofimov, G. Stelter and J. Schirmer.

[53] M. W. Schmidt, K. K. Baldridge, J. A. Boatz, S. T. Elbert, M. S. Gordon, J. H. Jensen, S. Koseki, N. Matsunaga, K. A. Nguyen, S. J. Su, T. L. Windus, M. Dupuis, J. A. Montgomery, J. Comput. Chem. 14 (1993) 1347.

[54] Direct ADC(4)/CVS one-particle Green's function code written by F. Tarantelli.

[55] Program written by M. F. Guest, J. H. van Lenthe, J. Kendrick, K. Schoffel, and P. Sherwood, with contributions from R. D. Amos, R. J. Buenker, M. Dupuis, N. C. Handy, I. H. Hiller, P. J. Knowles, V. Bonacic-Koutecky, W. von Niessen, R. J. Harrison, A. P. Rendell, V. R. Saunders, and A. J. Stone. Thepackage is derived from the original GAMESS code due to M. Dupuis, D. Spangler, and J. Wendoloski, NRCC Software Catalog, Vol. 1, Program No. QG01 (GAMESS), 1980.

[56] G. Schaftenaar, MOLDEN; CAOS/CAMM Center: The Netherlands, 2006.

[57] K. Siegbahn, C. Nordling, G. Johansson, J. Hedman, P.F. Heden, K. Hamrin, V. Gelius, T. Bergman, L.D.Werme, R. Manne, Y. Baer, ESCA Applied to Free Molecules, North-Holland, Amsterdam, 1969.

[58] N. T. Samuel, Chi-Ying Lee, L. J. Gamble, D. A. Fischer, and D. G. Castner, J. Electron Spectrosc. Relat. Phenom. 152 (2006) 134.

[59] M. Furukawa, H. Fujisawa, S. Katano, H. Ogasawara, Y. Kim, T. Komeda, A. Nilsson and M. Kawai, Surf. Sci. 532 (2003) 261.

TABLE 1 Energies Ω (eV) and relative oscillator strengths *f* of the vertical C 1s transitions of **thymine** calculated using the ADC(2)/6-31+G approach in comparison with the experimental data

Theory				Experiment	
Transition	Assignment [a]	Ω [b]	*f* [c]	Maximum	Ω [d]
1 ^{1}A"	C_8 1s → π_6*	284.50	0.342	A	284.9
2 ^{1}A"	C_7 1s → π_6*	286.02	0.639	B	285.9
3 ^{1}A"	C_9 1s → π_6*	286.45	0.004		
1 ^{1}A'	C_9 1s → 3s	286.53	0.063		
2 ^{1}A'	C_8 1s → 3s	286.86	< 0.001		
3 ^{1}A'	C_9 1s → 3p	287.46	0.092	C	287.3
4 ^{1}A"	C_8 1s → π_7* / 3p ?	287.54	0.209		
4 ^{1}A'	C_8 1s → 3p	287.71	0.015		
5 ^{1}A'	C_9 1s → 3p	287.85	0.101	D	287.8
5 ^{1}A"	C_9 1s → π_8* / 3p ?	287.88	0.181		
6 ^{1}A"	C_6 1s → π_6*	287.90	0.783		
6 ^{1}A'	C_8 1s → 3p	287.94	0.002		
7 ^{1}A"	C_8 1s → π_7* / 3p ?	288.10	< 0.001		
7 ^{1}A'	C_9 1s → 4s	288.43	0.137	E	288.4
8 ^{1}A'	C_7 1s → 3s	288.48	0.020		
9 ^{1}A'	C_8 1s → 4s	288.86	0.026		
8 ^{1}A"	C_9 1s → π_7* / 4p ?	288.95	0.032		
10 ^{1}A'	C_9 1s → 4p	288.97	0.039		
11 ^{1}A'	C_8 1s → 4p	289.03	0.024		
9 ^{1}A"	C_9 1s → π_8* / 4p ?	289.18	0.073		
12 ^{1}A'	C_8 1s → 4p	289.36	0.015		
10 ^{1}A"	C_8 1s → π_8* / 4p ?	289.38	< 0.001		
13 ^{1}A'	C_9 1s → 4p	289.46	0.017		
11 ^{1}A"	C_8 1s → π_8* / 4p ?	289.53	0.004		
12 ^{1}A"	C_9 1s → π_8* / 4p ?	289.61	0.005		
14 ^{1}A'	C_7 1s → 3p	289.66	0.033	F	289.4
13 ^{1}A"	C_5 1s → π_7*	289.68	1.000		
15 ^{1}A'	C_7 1s → 3p	289.83	0.010		
14 ^{1}A"	C_7 1s → π_7* / 3p ?	289.86	0.016		
16 ^{1}A'	C_8 1s → 5s	289.98	0.007		
15 ^{1}A"	C_7 1s → π_7* / 3p ?	290.04	0.062		
17 ^{1}A'	C_9 1s → 5s	290.06	0.079		
18 ^{1}A'	C_9 1s → 5p	290.30	0.091	G	290.7
16 ^{1}A"	C_8 1s → π_8*	290.33	0.175		
19 ^{1}A'	C_8 1s → 5p	290.34	0.013		
20 ^{1}A'	C_9 1s → 5p	290.48	0.006		
21 ^{1}A'	C_8 1s → 5p	290.48	0.017		

[a] Tentative assignment in terms of valence and Rydberg excitations; localization of core holes is shown in Fig. 1.

[b] The ADC(2) excitation energies have been corrected by −2.52 eV to compensate for a uniform error of the theoretical approach.

[c] The absolute oscillator strength of the strongest transition $C_5\,1s \rightarrow \pi_7^*$ ($13\,^1A''$) is 0.07098.

[d] Energies of the respective band maxima (Fig. 2).

TABLE 2 Energies Ω (eV) and relative oscillator strengths *f* of the vertical N 1s transitions of **thymine** calculated using the ADC(2)/6-31+G approach in comparison with the experimental data

Theory				Experiment	
Transition	Assignment [a]	Ω [b]	*f* [c]	Maximum	Ω [d]
1 ^{1}A"	N_4 1s → π_6*	401.47	1.000	A	401.7
2 ^{1}A"	N_3 1s → π_6*	401.84	0.719		
1 ^{1}A'	N_3 1s → 3s	402.02	0.669		
2 ^{1}A'	N_4 1s → 3s	402.44	0.580	B	402.7
3 ^{1}A"	N_4 1s → π_7* / 3p ?	402.52	0.295		
4 ^{1}A"	N_3 1s → π_7*	402.90	0.824		
3 ^{1}A'	N_4 1s → 3p	403.32	0.462		
4 ^{1}A'	N_3 1s → 3p	403.69	0.176	C	404.1
5 ^{1}A"	N_4 1s → π_7* / 3p ?	403.87	0.291		
5 ^{1}A'	N_4 1s → 3p	403.93	0.281		
6 ^{1}A'	N_3 1s → 3p	404.00	0.154		
6 ^{1}A"	N_3 1s → 3p / π_7* ?	404.06	0.180		
7 ^{1}A'	N_4 1s → 4s	404.38	0.063		
8 ^{1}A'	N_3 1s → 4s	404.95	0.101		
9 ^{1}A'	N_4 1s → 4p	405.01	0.035		
10 ^{1}A'	N_3 1s → 4p	405.22	0.218		
7 ^{1}A"	N_4 1s → π_8* / 4p ?	405.25	0.002		
11 ^{1}A'	N_4 1s → 4p	405.27	0.026		
12 ^{1}A'	N_3 1s → 4p	405.43	0.209		
8 ^{1}A"	N_3 1s → π_8* / 4p ?	405.50	0.002		
9 ^{1}A"	N_4 1s → π_8* / 4p ?	405.54	0.014		
13 ^{1}A'	N_4 1s → 5s	405.76	0.409	D	405.5
14 ^{1}A'	N_3 1s → 5s	405.87	0.311		
10 ^{1}A"	N_3 1s → π_8* / 5p ?	405.92	0.189		
15 ^{1}A'	N_4 1s → 5p	405.94	0.243		
16 ^{1}A'	N_4 1s → 5p	406.11	0.201		
17 ^{1}A'	N_3 1s → 5p	406.14	0.004		
11 ^{1}A"	N_4 1s → π_8*	406.37	0.974		

[a] Tentative assignment in terms of valence and Rydberg excitations; localization of core holes is shown in Fig. 1.

[b] The ADC(2) excitation energies have been corrected by −2.59 eV to compensate for a uniform error of the theoretical approach.

[c] The absolute oscillator strength of the strongest transition N_4 1s → π_6* (1 ^{1}A") is 0.01188.

[d] Energies of the respective band maxima (Fig. 3).

TABLE 3 Energies Ω (eV) and relative oscillator strengths *f* of the vertical O 1s transitions of **thymine** calculated using the ADC(2)/6-31+G approach in comparison with the experimental data

Theory				Experiment	
Transition	Assignment [a]	Ω [b]	*f* [c]	Maximum	Ω [d]
1 ^{1}A"	O_2 1s → π_6*	531.36	1.000	A	531.4
2 ^{1}A"	O_1 1s → π_7*	532.34	0.946	B	532.3
1 ^{1}A'	O_1 1s → 3s	534.33	0.004		
2 ^{1}A'	O_2 1s → 3s	534.48	0.013		
3 ^{1}A"	O_1 1s → π_6*	534.78	0.007		
3 ^{1}A'	O_1 1s → 3p	535.13	0.052	C	535.7
4 ^{1}A"	O_2 1s → π_7* / 3p ?	535.16	0.083		
4 ^{1}A'	O_2 1s → 3p	535.28	0.001		
5 ^{1}A'	O_2 1s → 3p	535.54	0.063		
5 ^{1}A"	O_2 1s → π_7* / 3p ?	535.56	0.019		
6 ^{1}A"	O_1 1s → 3p / π_7* ?	535.61	0.062		
6 ^{1}A'	O_1 1s → 3p	535.90	0.035		
7 ^{1}A'	O_2 1s → 4s	535.98	0.034		
8 ^{1}A'	O_1 1s → 3p	536.14	0.066		
9 ^{1}A'	O_2 1s → 4p	536.41	0.002		
10 ^{1}A'	O_2 1s → 4p	536.77	< 0.001	D	537.1
11 ^{1}A'	O_1 1s → 4s	536.78	0.012		
7 ^{1}A"	O_2 1s → π_8* / 4p ?	536.82	0.028		
8 ^{1}A"	O_2 1s → π_8* / 4p ?	537.07	0.011		
12 ^{1}A'	O_1 1s → 4p	537.19	0.031		
13 ^{1}A'	O_1 1s → 4p	537.19	0.032		
9 ^{1}A"	O_1 1s → π_8* / 4p ?	537.23	0.023		

[a] Tentative assignment in terms of valence and Rydberg excitations; localization of core holes is shown in Fig. 1.

[b] The ADC(2) excitation energies have been corrected by –2.19 eV to compensate for a uniform error of the theoretical approach.

[c] The absolute oscillator strength of the strongest transition $O_{2\,1s} \rightarrow \pi_6$* (1 ^{1}A") is 0.03097.

[d] Energies of the respective band maxima (Fig. 4).

TABLE 4 Energies Ω (eV) and intensities (*P*) of the lowest vertical core ionization transitions of **thymine** calculated using Hartree-Fock (HF) and ADC(4) approaches (basis set 6-31G) in comparison with the experimental data

Main configuration [a]	HF	ADC(4)		Experiment	
	Ω [b]	Ω [b]	*P*	Maximum	Ω [c]
$(C_8\ 1s)^{-1}$	304.88	290.67	0.57	A	291.0
$(C_9\ 1s)^{-1}$	304.04	290.95	0.64		
$(C_7\ 1s)^{-1}$	306.71	292.29	0.57	B	292.3
$(C_6\ 1s)^{-1}$	308.31	294.19	0.57	C	294.2
$(C_9\ 1s)^{-1}\ (6\ a'')^{-1}$		294.63	< 0.01		
$(C_8\ 1s)^{-1}\ (5\ a'')^{-1}$		295.01	< 0.01		
$(C_8\ 1s)^{-1}\ (6\ a'')^{-1}$		295.25	< 0.01		
$(C_5\ 1s)^{-1}$	309.42	295.36	0.59	D	295.2
$(C_7\ 1s)^{-1}\ (6\ a'')^{-1}$		295.60	0.01		
$(C_9\ 1s)^{-1}\ (5\ a'')^{-1}$		295.76	< 0.01		
$(N_4\ 1s)^{-1}$	423.97	406.52	0.59	A	406.7
$(N_3\ 1s)^{-1}$	424.31	406.80	0.58		
$(O_2\ 1s)^{-1}$	558.24	537.24	0.50	A	537.3
$(O_1\ 1s)^{-1}$	558.25	537.46	0.52		

[a] Only two-hole (2h) part of the two-hole one-particle (2h-1p) configuration is shown.

[b] The HF and ADC(4) ionization energies have been corrected by −1.90, −1.45 and −1.20 eV in case of C 1s, N 1s and O 1s ionization, respectively, to compensate for a uniform error of the theoretical approach.

[c] Energies of the respective band maxima (Figs. 5-7).

TABLE 5 Energies Ω (eV) and relative oscillator strengths *f* of the vertical C 1s transitions of **adenine** calculated using the ADC(2)/6-31+G approach in comparison with the experimental data

Theory				Experiment	
Transition	Assignment [a]	Ω [b]	*f* [c]	Maximum	Ω [d]
1 ^{1}A"	C_{10} 1s → π_6*	286.07	0.199	A'	~ 286.0
2 ^{1}A"	C_{10} 1s → π_7*	286.35	0.265	A	286.4
3 ^{1}A"	C_9 1s → $\pi_{6,7}$*	286.38	0.946		
4 ^{1}A"	C_7 1s → π_6*	286.74	0.877	B	286.8
5 ^{1}A"	C_6 1s → π_6*	287.37	1.000	C	287.4
1 ^{1}A'	C_{10} 1s → 3s	287.46	0.004		
6 ^{1}A"	C_8 1s → π_7*	287.46	0.972		
7 ^{1}A"	C_{10} 1s → π_9*	287.81	0.111	C'	~ 288.0
2 ^{1}A'	C_{10} 1s → 3p	288.03	0.014		
8 ^{1}A"	C_8 1s → π_6*	288.04	0.010		
9 ^{1}A"	C_9 1s → π_7*	288.21	0.021		
3 ^{1}A'	C_{10} 1s → 3p	288.46	0.005		
10 ^{1}A"	C_{10} 1s → π_8* / 3p ?	288.55	0.065		
4 ^{1}A'	C_7 1s → 3s	288.78	0.141		
5 ^{1}A'	C_{10} 1s → 4s	288.78	0.004		
6 ^{1}A'	C_{10} 1s → 4p	289.00	0.002	D	289.0
11 ^{1}A"	C_6 1s → π_7*	289.06	0.006		
7 ^{1}A'	C_9 1s → 3s	289.07	0.106		
8 ^{1}A'	C_8 1s → 3s	289.11	0.008		
9 ^{1}A'	C_{10} 1s → 4p	289.40	0.008		
12 ^{1}A"	C_7 1s → π_7* / 3p ?	289.54	0.005		
13 ^{1}A"	C_8 1s → π_9* / 3p ?	289.61	0.015		
10 ^{1}A'	C_9 1s → 3p	289.62	0.068		
14 ^{1}A"	C_{10} 1s → 4p ?	289.65	0.002		
11 ^{1}A'	C_7 1s → 3p	289.73	0.034		
12 ^{1}A'	C_8 1s → 3p	289.80	0.006		
13 ^{1}A'	C_7 1s → 3p	289.85	0.013		
14 ^{1}A'	C_9 1s → 3p	289.96	0.010		
15 ^{1}A'	C_6 1s → 3s	289.98	0.016		
16 ^{1}A'	C_{10} 1s → 5p	290.01	0.002		
17 ^{1}A'	C_{10} 1s → 5p	290.02	0.006		
15 ^{1}A"	C_{10} 1s → 5p ?	290.06	0.015		
16 ^{1}A"	C_9 1s → π_6* / 3p ?	290.07	0.037		
17 ^{1}A"	C_7 1s → π_8* / 3p?	290.14	0.009		
18 ^{1}A'	C_8 1s → 3p	290.25	0.000		
18 ^{1}A"	C_7 1s → π_9*	290.31	0.116		

TABLE 5 continued

Theory				Experiment	
Transition	Assignment [a]	Ω [b]	f [c]	Maximum	Ω [d]
19 ^{1}A'	C_{10} 1s → 6s	290.32	0.008		
19 ^{1}A"	C_8 1s → π_8* / 3p?	290.36	0.021		
20 ^{1}A'	C_9 1s → 4s	290.42	0.006		
20 ^{1}A"	C_9 1s → π_9* / 4p ?	290.56	0.054		
21 ^{1}A'	C_6 1s → 3p	290.63	0.009		
22 ^{1}A'	C_8 1s → 4s	290.69	0.013		
23 ^{1}A'	C_9 1s → 4p	290.73	0.001		
24 ^{1}A'	C_8 1s → 4p	290.74	0.016		

[a] Tentative assignment in terms of valence and Rydberg excitations; localization of core holes is shown in Fig. 1.

[b] The ADC(2) excitation energies have been corrected by −2.59 eV to compensate for a uniform error of the theoretical approach.

[c] The absolute oscillator strength of the strongest transition C_6 1s → π_6* (5 ^{1}A") is 0.05503.

[d] Energies of the respective band maxima (Fig. 8).

TABLE 6 Energies Ω (eV) and relative oscillator strengths *f* of the vertical N 1s transitions of **adenine** calculated using the ADC(2)/6-31+G approach in comparison with the experimental data

Theory				Experiment	
Transition	Assignment [a]	Ω [b]	*f* [c]	Maximum	Ω [d]
1 ^{1}A"	N_4 1s → π_6*	399.38	0.862	A	399.5
2 ^{1}A"	N_2 1s → π_6*	399.42	0.972		
3 ^{1}A"	N_5 1s → π_7*	399.64	1.000		
4 ^{1}A"	N_5 1s → π_6*	399.77	0.006		
5 ^{1}A"	N_4 1s → π_7*	400.69	0.082	A'	~ 400.4
1 ^{1}A'	N_5 1s → 3s	401.36	0.010	B'	401.0-401.3
2 ^{1}A'	N_3 1s → 3s	401.44	0.114		
3 ^{1}A'	N_4 1s → 3s	401.48	0.007		
6 ^{1}A"	N_3 1s → $\pi_{6,7}$*	401.50	0.303		
4 ^{1}A'	N_2 1s → 3s	401.58	0.003		
7 ^{1}A"	N_2 1s → π_7*	402.00	0.121	B	401.9
8 ^{1}A"	N_1 1s → $\pi_{6,7}$*	402.07	0.629		
5 ^{1}A'	N_5 1s → 3p	402.14	0.036		
6 ^{1}A'	N_5 1s → 3p	402.21	0.007		
7 ^{1}A'	N_4 1s → 3p	402.23	0.009		
8 ^{1}A'	N_2 1s → 3p	402.25	0.005		
9 ^{1}A'	N_1 1s → 3s	402.35	0.233		
9 ^{1}A"	N_5 1s → 3p	402.36	0.021		
10 ^{1}A'	N_4 1s → 3p	402.44	0.031		
11 ^{1}A'	N_2 1s → 3p	402.44	0.030		
10 ^{1}A"	N_4 1s → 3p	402.47	0.059		
11 ^{1}A"	N_2 1s → 3p	402.58	0.090		
12 ^{1}A'	N_5 1s → 4s	402.65	0.014		
12 ^{1}A"	N_2 1s → π_8*	402.84	0.027	C	403.0
13 ^{1}A'	N_3 1s → 4p	402.85	0.480		
14 ^{1}A'	N_4 1s → 4s	402.87	0.005		
13 ^{1}A"	N_4 1s → π_8*	403.03	0.049		
15 ^{1}A'	N_5 1s → 4p	403.09	0.009		
16 ^{1}A'	N_4 1s → 4p	403.13	0.003		
17 ^{1}A'	N_5 1s → 4p	403.14	0.004		
14 ^{1}A"	N_3 1s → 4p	403.27	0.006		
15 ^{1}A"	N_5 1s → 4p	403.29	0.001		
18 ^{1}A'	N_2 1s → 4s	403.33	0.007		
19 ^{1}A'	N_3 1s → 4p	403.37	0.026		
16 ^{1}A"	N_1 1s → π_7*	403.40	0.070		
20 ^{1}A'	N_4 1s → 4p	403.47	0.030		
17 ^{1}A"	N_3 1s → π_8*	403.66	0.152		

TABLE 6 continued

Theory				Experiment	
Transition	Assignment [a]	Ω [b]	f [c]	Maximum	Ω [d]
21 ^{1}A'	N_2 1s → 4p	403.71	0.004		
22 ^{1}A'	N_2 1s → 4p	403.74	0.023		
18 ^{1}A"	N_5 1s → π_8*	403.76	0.023		
19 ^{1}A"	N_4 1s → 4p	403.81	0.013		
23 ^{1}A'	N_5 1s → 5s	403.86	0.002		
24 ^{1}A'	N_4 1s → 5s	403.98	0.007		
20 ^{1}A"	N_5 1s → π_9*	404.00	0.037		

[a] Tentative assignment in terms of valence and Rydberg excitations; localization of core holes is shown in Fig. 1.

[b] The ADC(2) excitation energies have been corrected by −2.39 eV to compensate for a uniform error of the theoretical approach.

[c] The absolute oscillator strength of the strongest transition N_5 1s → π_7* (3 ^{1}A") is 0.03555.

[d] Energies of the respective band maxima (Fig. 9).

TABLE 7 Energies Ω (eV) and intensities (*P*) of the lowest vertical core ionization transitions of **adenine** calculated using Hartree-Fock (HF) and ADC(4) approaches (basis set 6-31G) in comparison with the experimental data

Main configuration	HF	ADC(4)		Experiment	
	Ω [a]	Ω [a]	*P*	Maximum	Ω [b]
$(C_{10}\ 1s)^{-1}$	305.12	291.19	0.58	A	291.0
$(C_9\ 1s)^{-1}$	306.54	291.94	0.54	B	292.5
$(C_8\ 1s)^{-1}$	306.86	292.47	0.57		
$(C_7\ 1s)^{-1}$	306.90	292.66	0.52		
$(C_6\ 1s)^{-1}$	307.41	292.96	0.56		
$(N_5\ 1s)^{-1}$	422.04	404.27	0.53	A	404.4
$(N_4\ 1s)^{-1}$	422.27	404.40	0.51		
$(N_2\ 1s)^{-1}$	422.57	404.99	0.54		
$(N_3\ 1s)^{-1}$	422.47	405.62	0.58	B	405.7
$(N_1\ 1s)^{-1}$	423.99	406.63	0.57	C	406.7

[a] The HF and ADC(4) ionization energies have been corrected by −1.61 and −1.62 eV in case of the C 1s and N 1s ionization, respectively, to compensate for a uniform error of the theoretical approach.

[b] Energies of the respective band maxima (Figs. 10-11).

Figure captions.

Fig. 1. (a) Schematic representation of thymine and adenine. The numbering of the atoms reflects the HF energetical order of the respective core-hole orbitals; π* orbital electron densities (view from top) of thymine (b) and adenine (c).

Fig. 2 Experimental and calculated C 1s NEXAFS spectra of thymine. The theoretical spectral envelope has been constructed by convoluting the calculated absorption spectrum with Lorenzians of 0.4 eV FWHM and shifting the spectrum as a whole by –2.52 eV.

Fig. 3. Experimental and calculated N 1s NEXAFS spectra of thymine. The theoretical spectral envelope has been constructed by convoluting the calculated absorption spectrum with Lorentzians of 0.6 eV FWHM and shifting the spectrum as a whole by –2.59 eV.

Fig. 4. Experimental and calculated O 1s NEXAFS spectra of thymine. The theoretical spectral envelope has been constructed by convoluting the calculated absorption spectrum with Lorenzians of 0.8 eV FWHM and shifting the spectrum as a whole by –2.19 eV.

Fig. 5. Experimental and calculated C 1s XPS spectra of thymine. The theoretical spectral envelope has been constructed by convoluting the calculated absorption spectrum with Lorenzians of 0.5 eV FWHM and shifting the spectrum as a whole by –1.90 eV.

Fig. 6. Experimental and calculated N 1s XPS spectra of thymine. The theoretical spectral envelope has been constructed by convoluting the calculated absorption spectrum with Lorenzians of 0.7 eV FWHM and shifting the spectrum as a whole by –2.20 eV.

Fig. 7. Experimental and calculated O 1s XPS spectra of thymine. The theoretical spectral envelope has been constructed by convoluting the calculated absorption spectrum with Lorenzians of 0.7 eV FWHM and shifting the spectrum as a whole by –1.20 eV.

Fig. 8. Experimental and calculated C 1s NEXAFS spectra of adenine. The theoretical spectral envelope has been constructed by convoluting the calculated absorption spectrum with Lorenzians of 0.4 eV FWHM and shifting the spectrum as a whole by –2.59 eV.

Fig. 9. Experimental and calculated N 1s NEXAFS spectra of adenine. The theoretical spectral envelope has been constructed by convoluting the calculated absorption spectrum with Lorenzians of 0.5 eV FWHM and shifting the spectrum as a whole by –2.39 eV.

Fig. 10. Experimental and calculated C 1s XPS spectra of adenine. The theoretical spectral envelope has been constructed by convoluting the calculated absorption spectrum with Lorenzians of 0.5 eV FWHM and shifting the spectrum as a whole by –1.61 eV.

Fig. 11. Experimental and calculated N 1s XPS spectra of adenine. The theoretical spectral envelope has been constructed by convoluting the calculated absorption spectrum with Lorenzians of 0.6 eV FWHM and shifting the spectrum as a whole by –1.62 eV.

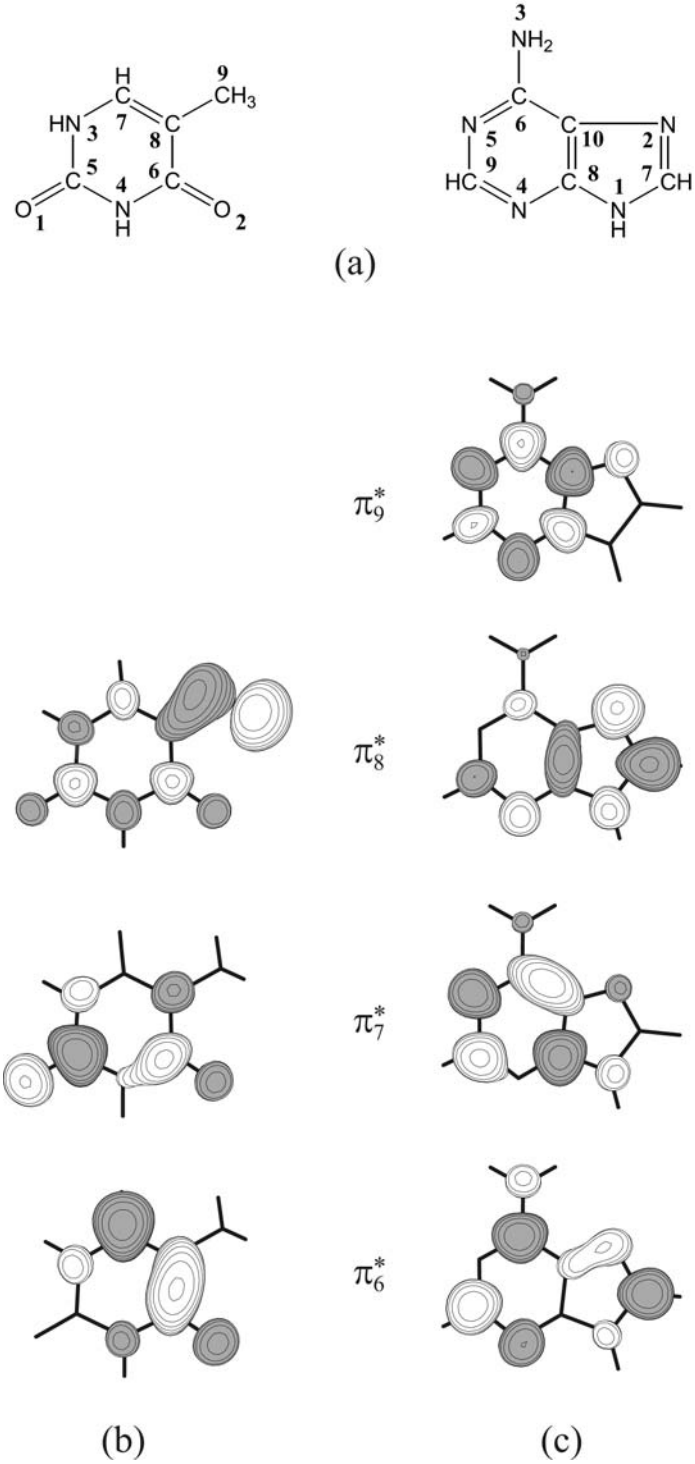

Fig. 1. (a) Schematic representation of thymine and adenine. The numbering of the atoms reflects the HF energetical order of the respective core-hole orbitals; π* orbital electron densities (view from top) of thymine (b) and adenine (c).

Fig. 1

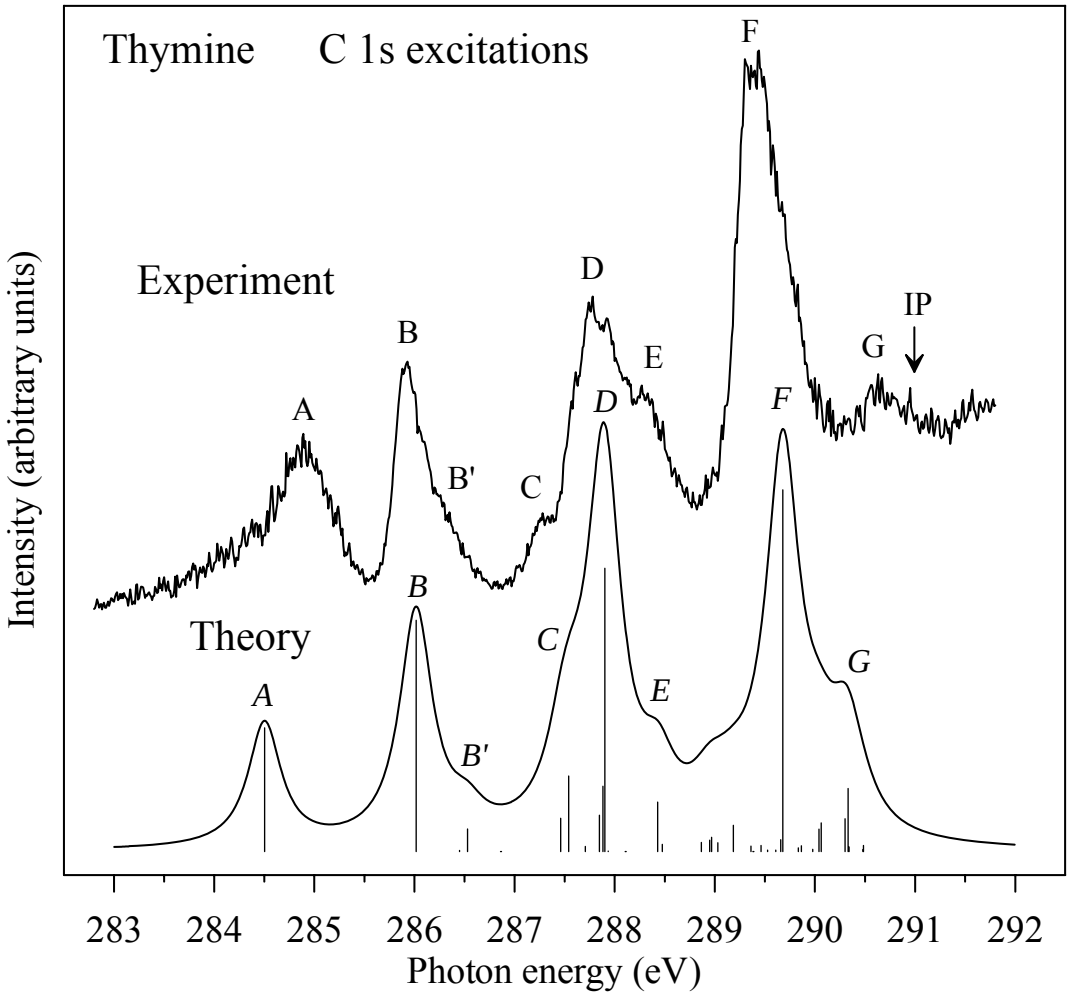

Experimental and calculated C 1s NEXAFS spectra of thymine. The theoretical spectral envelope has been constructed by convoluting the calculated absorption spectrum with Lorenzians of 0.4 eV FWHM and shifting the spectrum as a whole by –2.52 eV.

Fig. 2

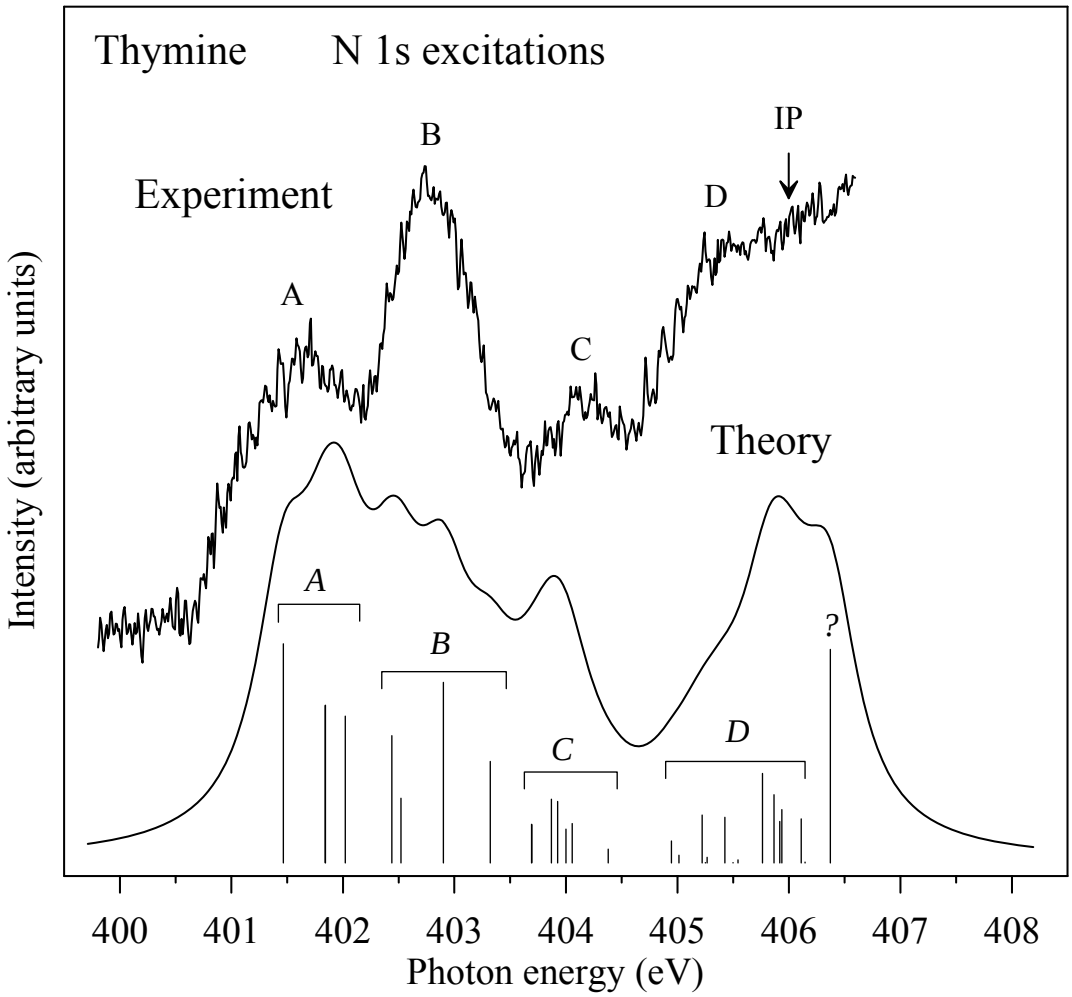

Experimental and calculated N 1s NEXAFS spectra of thymine. The theoretical spectral envelope has been constructed by convoluting the calculated absorption spectrum with Lorenzians of 0.6 eV FWHM and shifting the spectrum as a whole by –2.59 eV.

Fig. 3

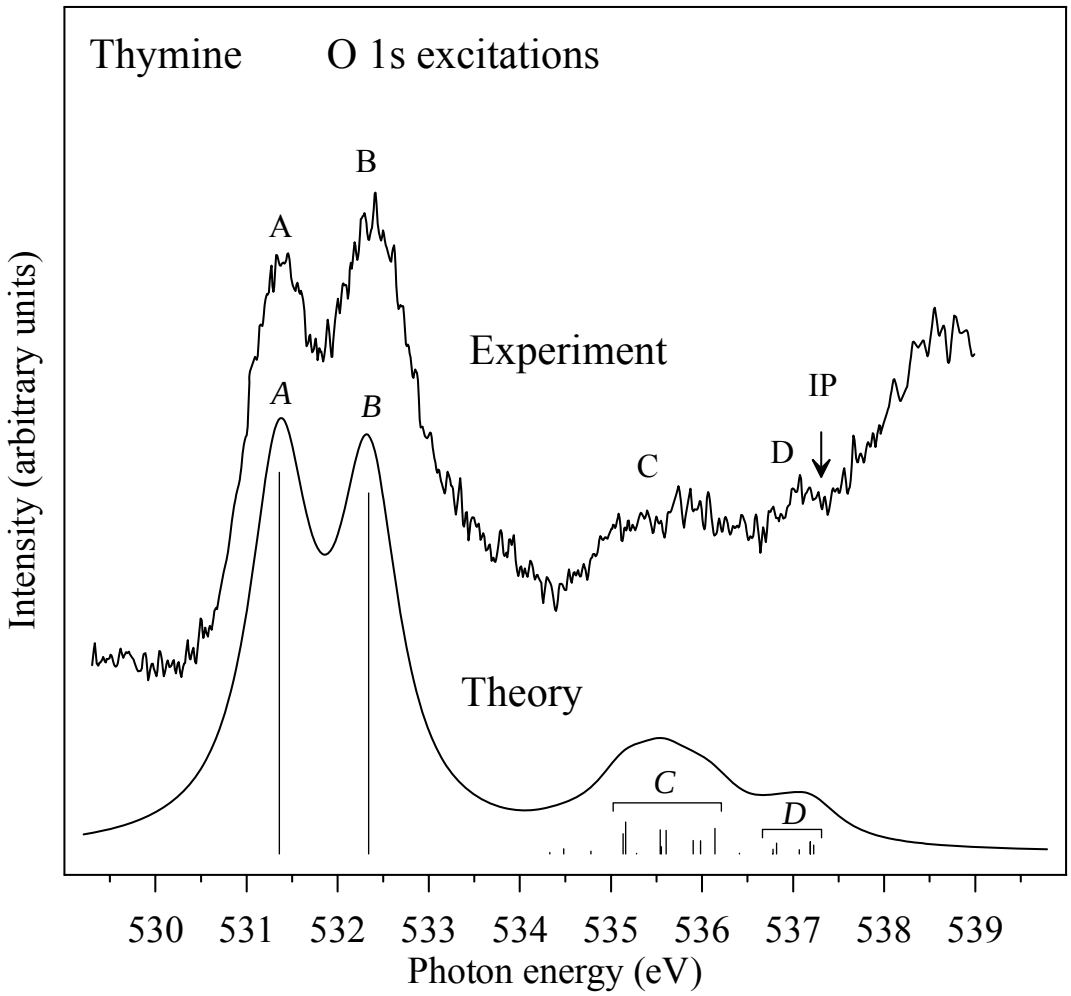

Experimental and calculated O 1s NEXAFS spectra of thymine. The theoretical spectral envelope has been constructed by convoluting the calculated absorption spectrum with Lorenzians of 0.8 eV FWHM and shifting the spectrum as a whole by –2.19 eV.

Fig. 4

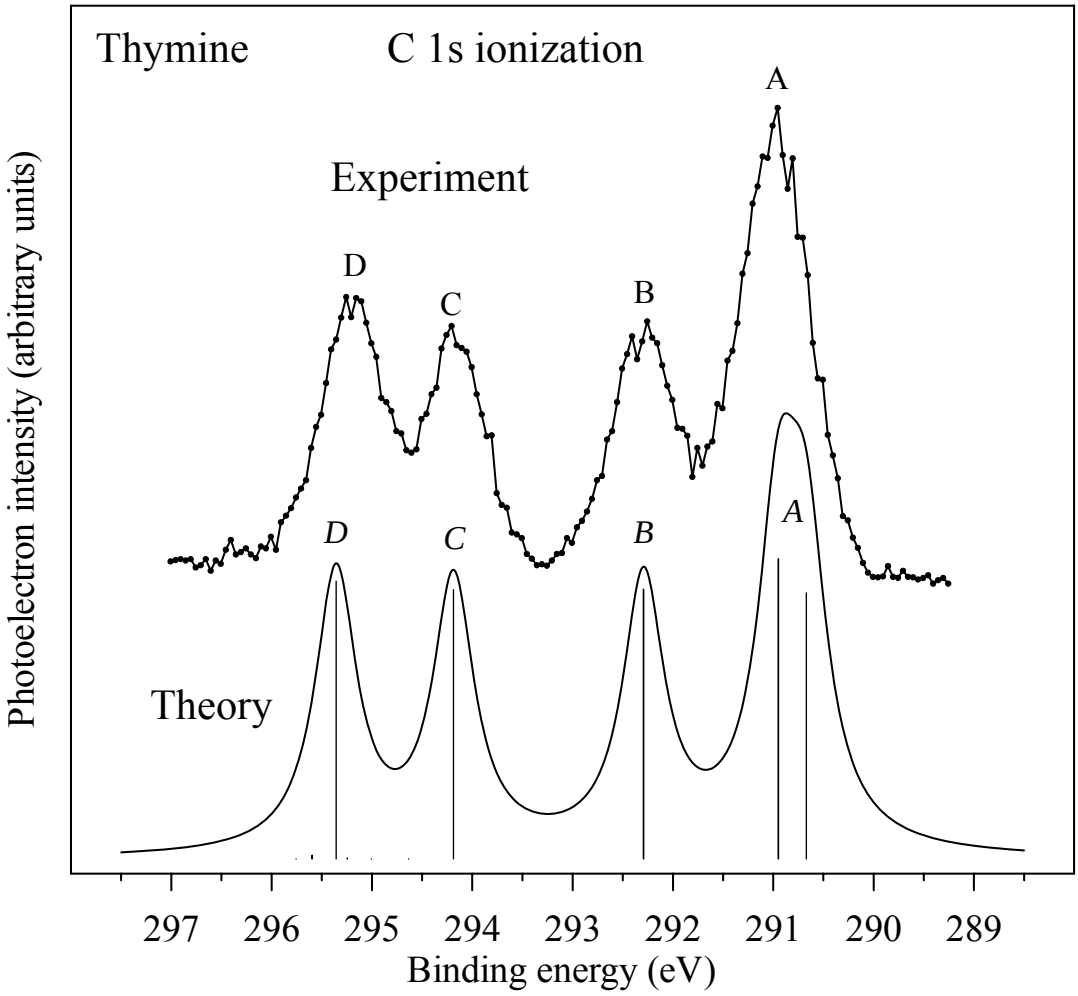

Experimental and calculated C 1s XPS spectra of thymine. The theoretical spectral envelope has been constructed by convoluting the calculated absorption spectrum with Lorenzians of 0.5 eV FWHM and shifting the spectrum as a whole by –1.90 eV.

Fig. 5

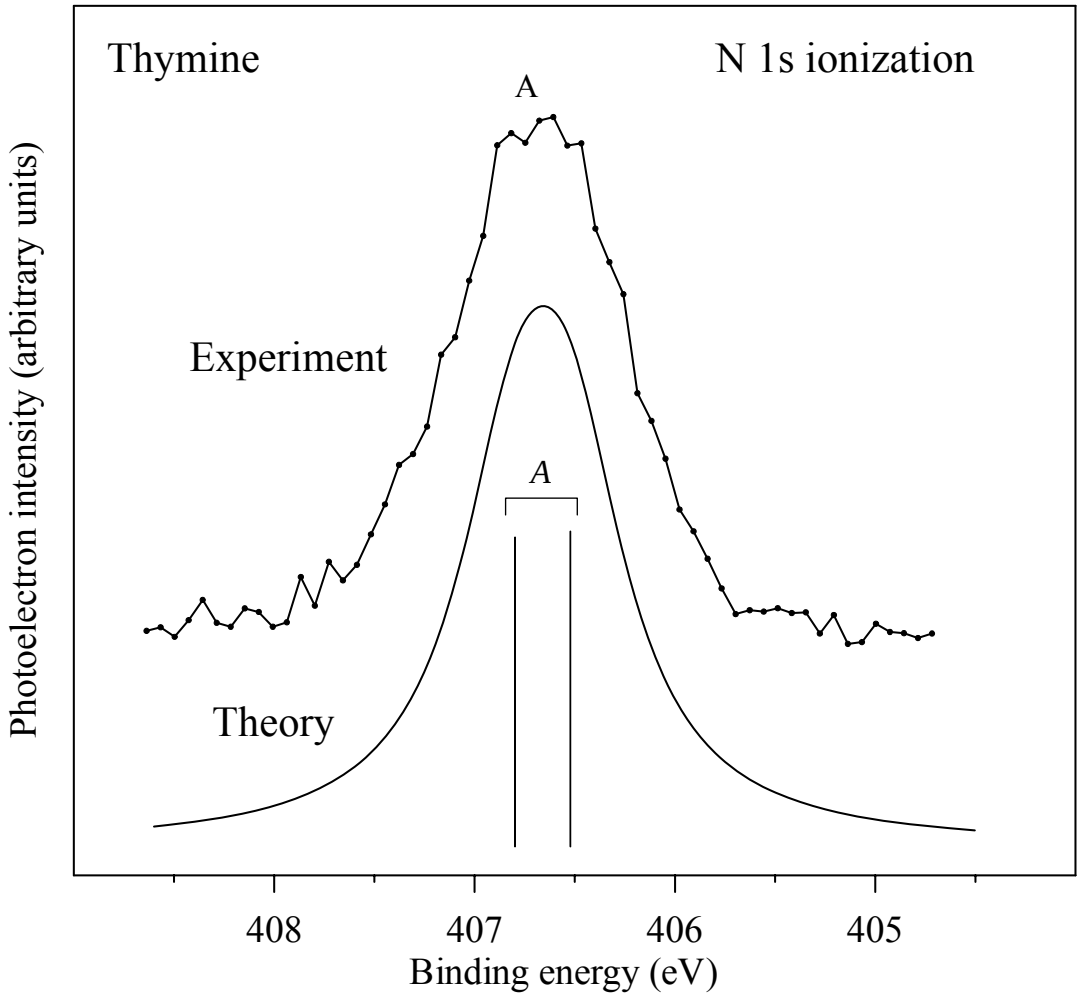

Experimental and calculated N 1s XPS spectra of thymine. The theoretical spectral envelope has been constructed by convoluting the calculated absorption spectrum with Lorenzians of 0.7 eV FWHM and shifting the spectrum as a whole by −1.45 eV.

Fig. 6

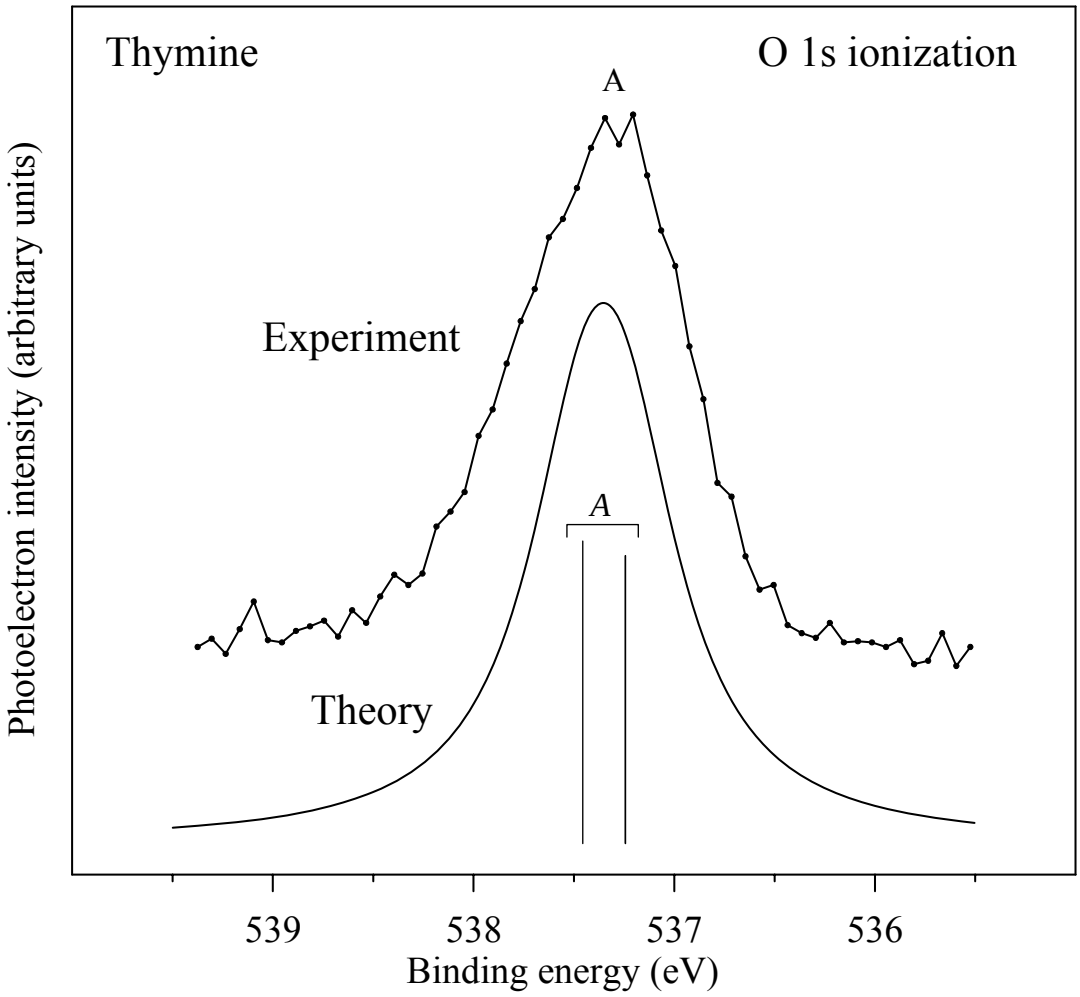

Experimental and calculated O 1s XPS spectra of thymine. The theoretical spectral envelope has been constructed by convoluting the calculated absorption spectrum with Lorenzians of 0.7 eV FWHM and shifting the spectrum as a whole by −1.20 eV.

Fig. 7

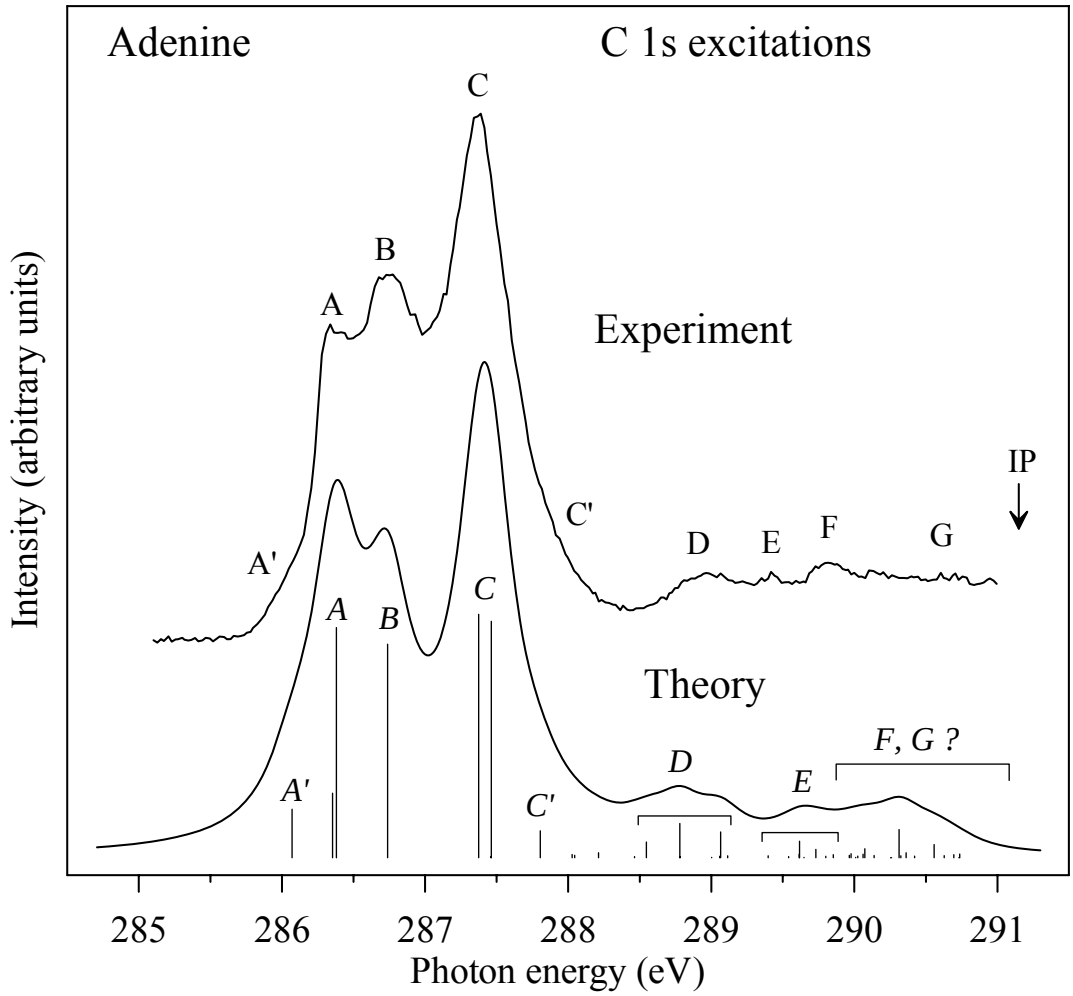

Experimental and calculated C 1s NEXAFS spectra of adenine. The theoretical spectral envelope has been constructed by convoluting the calculated absorption spectrum with Lorenzians of 0.4 eV FWHM and shifting the spectrum as a whole by –2.59 eV.

Fig. 8

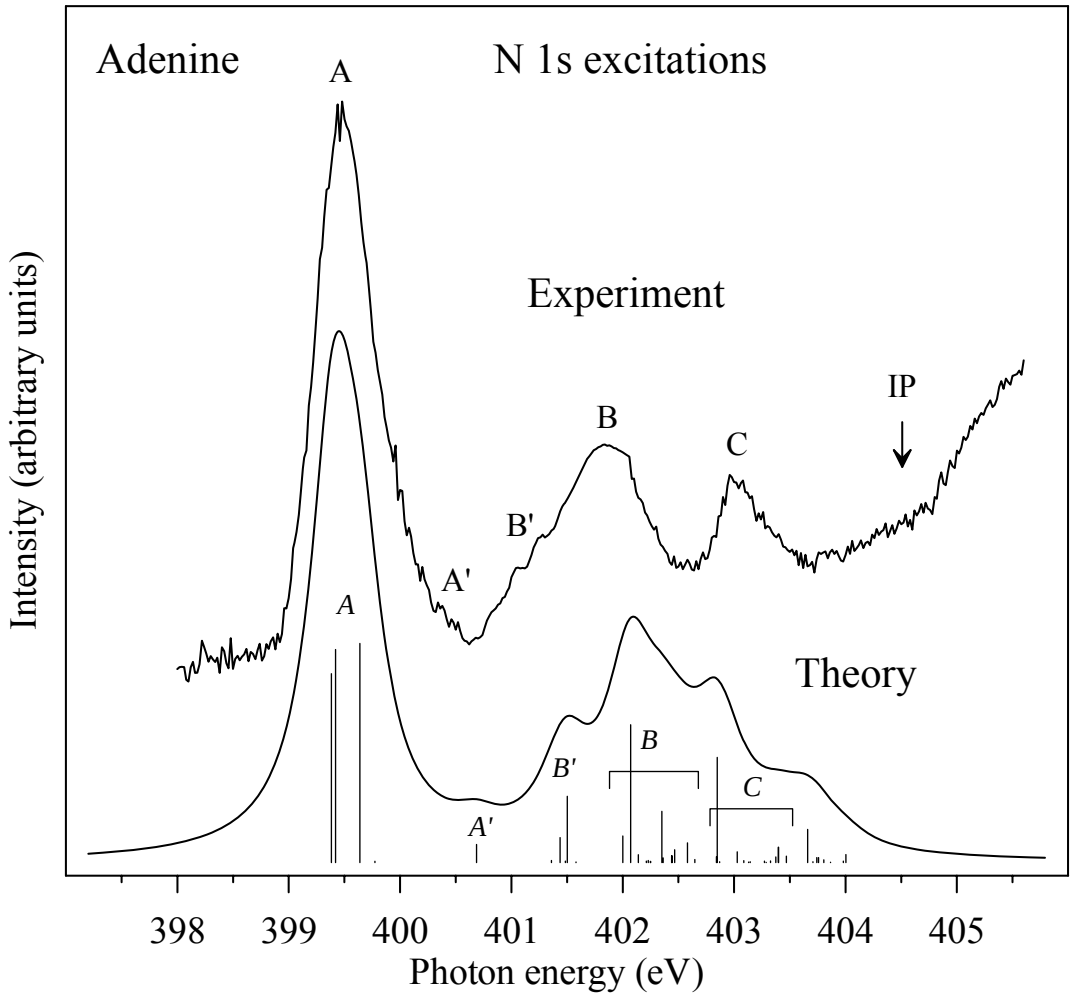

Experimental and calculated N 1s NEXAFS spectra of adenine. The theoretical spectral envelope has been constructed by convoluting the calculated absorption spectrum with Lorenzians of 0.5 eV FWHM and shifting the spectrum as a whole by –2.39 eV.

Fig. 9

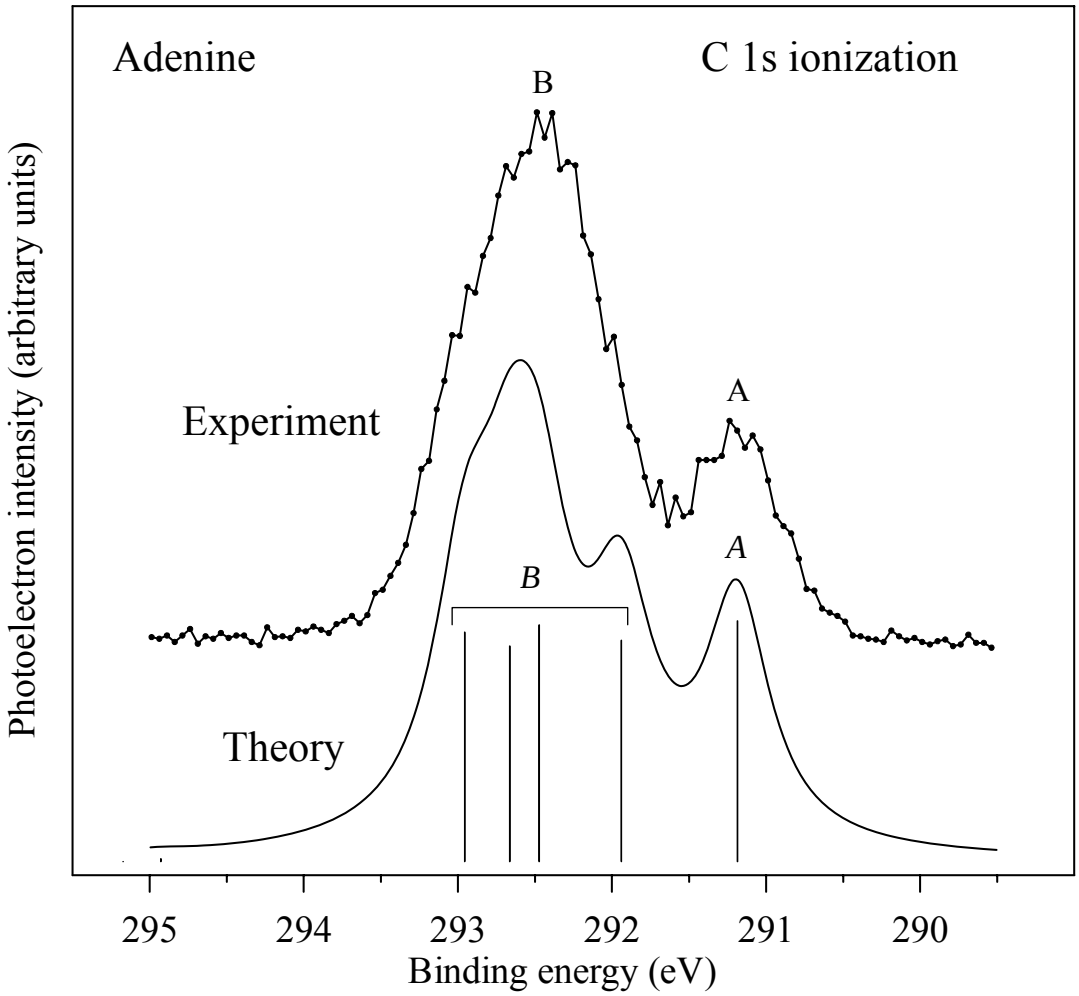

Experimental and calculated C 1s XPS spectra of adenine. The theoretical spectral envelope has been constructed by convoluting the calculated absorption spectrum with Lorenzians of 0.5 eV FWHM and shifting the spectrum as a whole by –1.61 eV.

Fig. 10

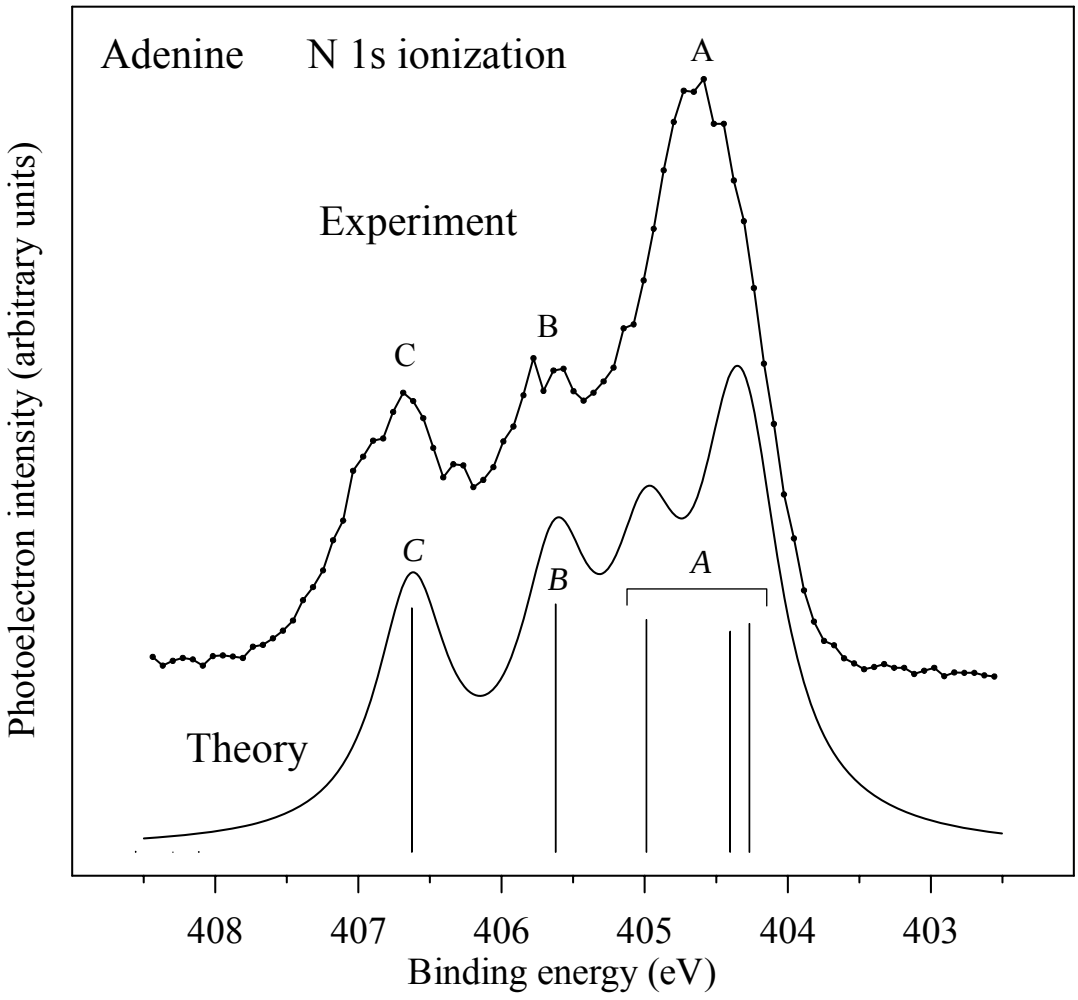

Experimental and calculated N 1s XPS spectra of adenine. The theoretical spectral envelope has been constructed by convoluting the calculated absorption spectrum with Lorenzians of 0.6 eV FWHM and shifting the spectrum as a whole by –1.62 eV.

Fig. 11